

Lake Okaro: Explosions and Erosion

A study into erosion on the hills to the north of Lake Okaro and the 0.7 ka phreatic and hydrothermal eruptions at Lake Okaro to help understand the current geomorphology



**Lyndon Hardy
BSc(Hons) Thesis
University of Otago
2005**

Table Of Contents

1	Abstract.....	4
2	Introduction.....	5
2.1	Previous Work and Generalised Geological Setting.....	6
2.1.1	Sedimentary Response in Volcanic Settings.....	8
2.1.2	Hydrothermal Eruptions.....	9
2.2	Methodology and Fieldwork.....	14
2.2.1	GPS Mapping and Rill Analysis.....	15
2.2.2	Grainsize Analysis.....	15
2.2.3	X-Ray Diffraction.....	17
2.2.4	Cathodoluminescence and Electron Microprobe Analysis.....	17
3	Erosion Rills North of Lake Okaro.....	19
3.1.1	GPS Mapping of Rills.....	19
3.1.2	Rill Depth.....	21
3.1.3	Interpretation and Discussion.....	23
4	Lake Okaro Eruptions.....	26
4.1	Breccia Description and Analysis.....	26
4.1.1	Okaro-A.....	26
4.1.2	Okaro-B.....	31
4.1.3	Okaro-C.....	36
4.2	Distribution and Volume.....	40
4.3	Interpretation.....	40
4.3.1	Eruption episodes.....	40
4.3.2	Eruption mechanism.....	42
4.3.3	Summary.....	43
5	Discussion.....	44
6	Conclusions.....	47
7	References.....	48
8	Appendices.....	51
8.1	Appendix A – Okaro-Area Location Map.....	51
8.2	Appendix B – Okaro-Area Base Map.....	52
8.3	Appendix C – Outcrop and Sample Data.....	53
8.4	Appendix D – Auger Hole Data & Locations.....	56
8.5	Appendix E – Grainsize Analysis Data.....	57
8.6	Appendix F – X-Ray Diffraction Data Summary.....	60
8.7	Appendix G – Electron Microprobe Analysis Data.....	61
8.8	Appendix H – Composite Measured Section Through Okaro-Breccia.....	62
8.9	Appendix I – Schematic Interpretation of Eruption for the Okaro-A and -B Deposits and the Formation of Lake Okaro.....	63
8.10	Appendix J – Paleogeographic Interpretation of the Area Now Occupied by Lake Okaro.....	66

List of Figures

Figure 1	Lake shoreline sketch diagram	6
Figure 2	Structural interpretation of area	9
Figure 3	Lake Okaro bathymetry	13
Figure 4	Schematic cross-section for crater	14
Figure 5	Rill complexity rating scale	19
Figure 6	Panorama of studied valleys	20
Figure 7	GPS-derived rill map	20
Figure 8	Thickness of Rotomahana Mud along baseline	21
Figure 9	Rill/Inter-rill thickness	22
Figure 10	In-filled channel cutting through AD1886 paleosol	22
Figure 11	Rills in Rotomahana Mud 17 days after AD1886 eruption	24
Figure 12	Okaro-A and Okaro-B above Kaharoa Ash	27
Figure 13	Okaro-A grainsize histograms	29
Figure 14	Quartz cathodoluminescence images	30
Figure 15	Ternary diagram for electron microprobe data	31
Figure 16	Rangitaiki Ignimbrite ejecta block with bomb sag in Okaro-B	32
Figure 17	Hydrothermal quartz in plane polarised light	33
Figure 18	Okaro-B grainsize histograms	34
Figure 19	Okaro-C below AD1886 paleosol and Rotomahana Mud	37
Figure 20	Okaro-C grainsize histograms	39
Figure 21	Altered feldspars in cross polarised light	39

List of Tables

Table 1	Stratigraphy from Environment Bay of Plenty drill hole	8
Table 2	Okaro-A grainsize statistics	28
Table 3	Electron microprobe analysis data	30
Table 4	Okaro-B grainsize statistics	34
Table 5	Okaro-C grainsize statistics	38

Acknowledgements

Thanks must be given to my supervisor, Dr James White, for putting up with many inane questions, theories and ideas, as well as giving me vital feedback and direction. Thanks also go to Ray Marx, for his help with grain size analysis methodology and knowledge of the area, Vern Manville and Geoff Kilgour, for help with Coulter grainsize analysis, Dr Lorraine Paterson, for help with cathodoluminescence and quantitative glass analysis, and Dr J. Michael Palin, for helping understand the data generated from the electron microprobe. Thanks go to landowners in the Okaro area: Shane Birchill allowed me repeated access to his property, as did the Lynseys, and Murray Travers was good enough to let me dirty his brand new extension ladder for the measured section; cheers, all. Cheers as well to the poor souls sharing the 4th year room with me... we had some fun during the year. And last, but definitely not least, thanks go to my wife, Melissa, for putting up with another year apart so that I could get this finished.

1 Abstract

Lake Okaro was formed approximately 700 years ago, simultaneous with a late stage of the Kaharoa eruptive phase at Tarawera, in a phreatic eruption that induced a number of secondary hydrothermal eruptions. The phreatic eruption was initiated within or beneath the welded Rangitaiki Ignimbrite and involved the excavation of a crater at least 80-metres deep at the south end of the present lake, with the resulting ejecta creating a 'cap' over an area of previous hydrothermal activity now occupied by the north end of the lake. I infer that increases in pressure as a result of the hydrothermal system being buried by material from the phreatic eruption led to a number of shallowly focused (<60 metres depth) hydrothermal eruptions, which helped fill the phreatic eruption crater, making the lake its present shape. Slumping into the craters, in addition to redeposition of Kaharoa tephra and AD1886 Rotomahana Mud from the surrounding hills, filled the lake to its present observed depth, with deep points indicating the position of original craters.

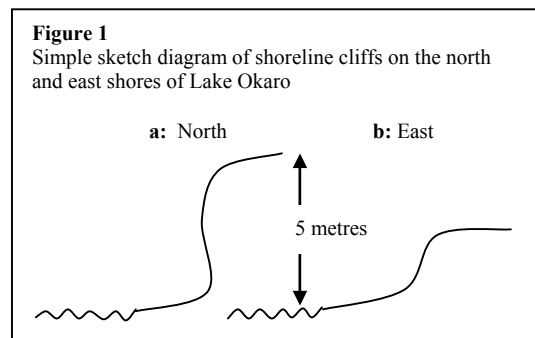
Erosion rills scarring hillsides to the north of Lake Okaro occur entirely within the Rotomahana Mud and represent part of the immediate sedimentary response to the AD1886 eruption. Increased sediment flow from erosion of the Rotomahana Mud over a low-permeability soil horizon developed in the Okaro Deposit initially caused degradation of valley floors, but once the rills stabilised and the sediment flow decreased, aggradation rates of approximately 0.013 metres/year occurred raising the valley floors 0.10 metres higher than their pre-eruption level by 1917, when the Frying Pan Flat hydrothermal eruption at Waimangu deposited a layer of material over the area.

2 Introduction

Lake Okaro occupies a small basin surrounded by ejecta formed by explosive activity, and is in an area buried by up to 1 metre of Rotomahana Mud during the AD1886 eruption. This report examines the nature of the eruptions of Lake Okaro, and also the erosional modification of the Rotomahana Mud north of the lake, where it is the thickest.

Lake Okaro (see Appendix A for detailed map) is located toward the southern margin of the Okataina Volcanic Complex, within the Taupo Volcanic Zone. Approximately 1200 metres north is Waimangu, which is situated at the southern end of the AD1886 Tarawera eruption rift, and 2 kilometres south of the lake is Maungakakamea (Rainbow Mountain). The lake is roughly 20 kilometres south-southeast of Rotorua, and is accessible via the Waimangu Road from State Highway 5 and the Okaro Road from State Highway 38. Tourists frequently travel the road on the way to Waimangu, and the lake itself is a destination for water skiing and fishing (algal-blooms permitting). The land surrounding the lake has been intensively farmed since the late 1950s (Cross, 1963), and the lake itself is currently the focus of efforts by Environment Bay of Plenty and Waikato University to control phosphorus and nitrogen influx in order to reduce algal pollution of the lake (McIntosh, 2003).

The lake itself has a 500- by 700-metre north-south elongate ovoid shape and a maximum depth of 18 metres (Irwin 1974). The south end has tree-covered cliffs rising approximately 20 metres above lake-level, while the east side (Figure 1b) has a 2 metre high cliff cut into Okaro Breccia behind a platform sloping gently upward from present lake level. The lakes' catchment extends to the northwest, whilst the outlet is to the southeast. There is an approximately 50-metre breach in the eastern terrace where the outlet stream occurs. The north end of the lake has cliffs of Earthquake Flat Pyroclastics with a maximum height of 5 metres, which are gently undercut to ~3 metres above present lake level (Figure 1a). The Okaro Road runs along the west side of the lake, and that shore has undergone extensive modification and landscaping, and the original shoreline is no longer observable except in the southwest corner, which also has tall (~20 metre) cliffs where slumping of the road into



the lake has been a problem over recent years (Ray Marx, personal communications 2005).

The following report is divided into two main sections:

- 1) An investigation into the Okaro Breccia deposits in order to determine a likely sequence of events. This will then allow estimation of the size of the eruption, which in turn will allow assessment of the level of hazard associated with the event;
- 2) Investigations into erosion features on hillsides to the north of Lake Okaro, in order to better understand controls on the nature, intensity, and duration of the immediate sedimentary response to the AD1886 Rotomahana/Tarawera eruptions.

These two topics will enhance understanding of the recent geomorphological processes affecting Lake Okaro and the immediate surroundings in an active hydrothermal and volcanic area adjacent to the Okataina Volcanic Complex.

2.1 Previous Work and Generalised Geological Setting

Lake Okaro has been mapped previously as an explosion crater (Grange, 1937), and as a hydrothermal eruption crater (Nairn, 2002); its oval shape and the surrounding breccia certainly suggests an explosive origin. The area around Lake Okaro has been mapped based on the topography forming unit, which in this case is the Earthquake Flat Pyroclastics, a 65,000-year-old series of weakly compacted ash and pumice flows with an origin approximately 6 km northwest of Okaro (Nairn, 2002). The Earthquake Flat Pyroclastics is not the local basement, nor is it the only volcanic deposit as it is overlain by between 2 and 5 metres of younger tephra fall deposits from numerous eruptions from the Okataina Volcanic Complex, as well as from Taupo Volcano some 80 kilometres to the south, during the intervening time, and is variably mantled (~1 metre in the north to ~0.1 metres in the south) by the Rotomahana Mud from the AD1886 Tarawera eruption.

The Earthquake Flat Pyroclastics are weakly compacted crystal-rich (~50% by visual estimate) lapilli-bearing ash with large blocks of coarse, vesicular pumice, with large (up to 5 mm) quartz, plagioclase, hornblende, and biotite phenocrysts. In the Okaro area it has a total thickness greater than 50 metres and occurs as a series of individual flow units, each between 1.2 and 2.5 metres thick; millimetre to centimetre scale reworking of material is evident between units, suggesting at least some time between individual eruptions. It has a very poorly sorted, matrix with platykurtic distribution and a graphic mean of 1.27λ (after Folk, 1980; see Appendix E for full grainsize data).

Lake Okaro: Explosions and Erosion

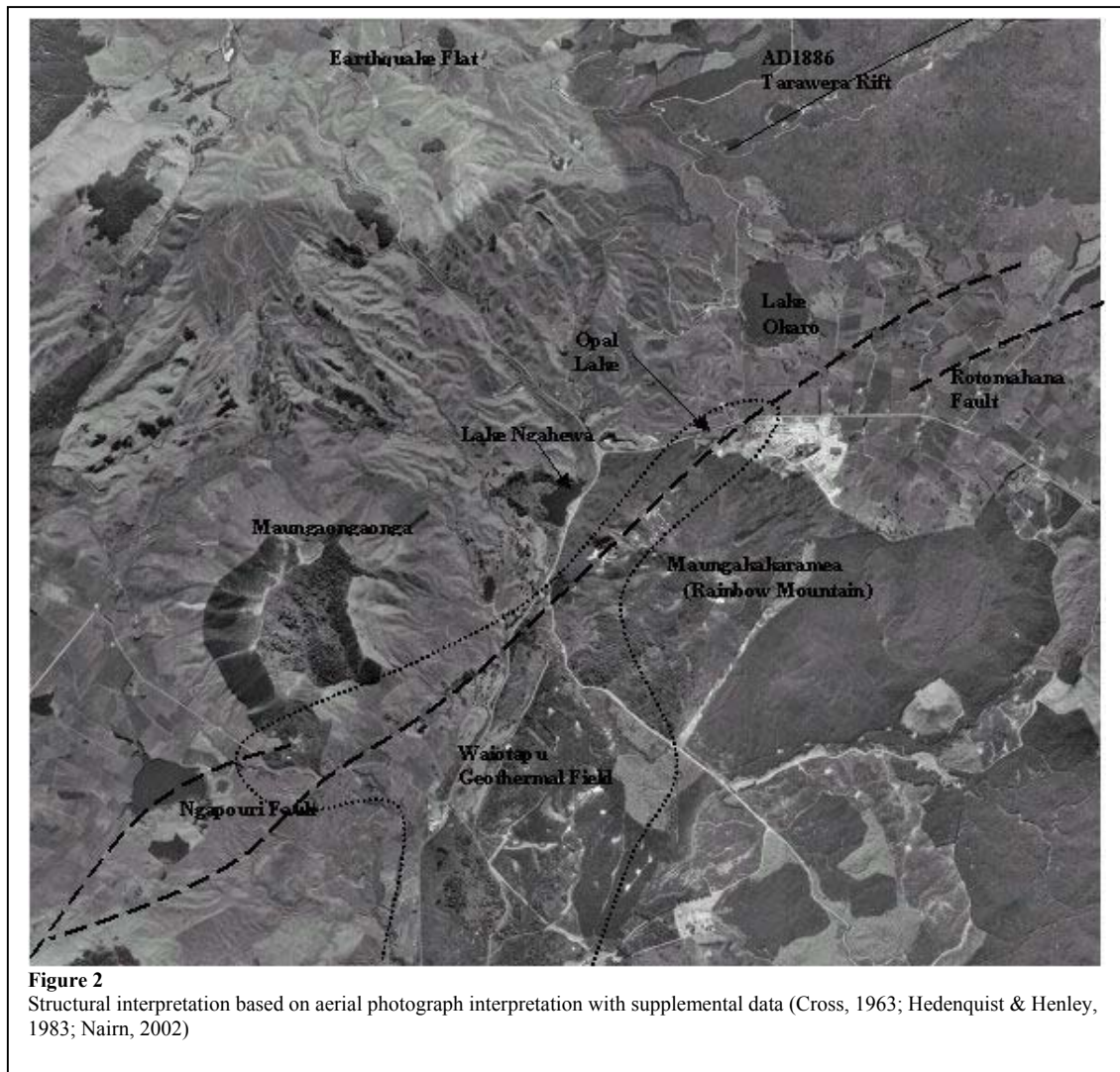
The Rotomahana Mud is an uncompacted grey mud-sand grade pyroclastic deposit erupted through the old Rotomahana geothermal system during the AD1886 Tarawera eruption (Rosseel, 2002). The eruption was driven by a basaltic dyke intruded to feed a series of *en echelon* fissures for a length of 17 kilometres (Nairn, 2002). Where rising basalt interacted the Rotomahana geothermal field, a phreatomagmatic eruption ensued ejecting $\sim 0.5 \text{ km}^3$ of rock and mud (Simmons et al, 1993).

A drill hole put down near Lake Okaro (Table 1) by Environment Bay of Plenty showed the Earthquake Flat Pyroclastics to be approximately 50 metres thick, with 10 metres of distal Rotoiti Pyroclastics and 7 metres of Rangitaiki Ignimbrite underlying it (Nairn, 2003). Nairn (2003) noted that the RI was much thinner than expected, because more than 100 metres is exposed on the caldera rim at Lake Rotomahana roughly 3 km to the northeast (Nairn, 2002). Warm water was encountered at approximately 40 metres depth within the well (Shane Burchell, pers. comms. 2005).

Table 1
Stratigraphy from water supply well drilled at Lake Okaro by Environment Bay of Plenty (adapted from Nairn, 2003).

Metres below ground	Unit
0-6 m	Okaro hydrothermal eruption breccia
6-56.6 m	Earthquake Flat Pyroclastics
56.6-65.6 m	Rotoiti Pyroclastics (distal facies), and crystal-poor silts
65.6-72 m	Rangitaiki Ignimbrite
72-80 m	Siltstones, some carbonaceous
80m	Base of hole

The area has a number of northeast trending faults (Figure 2, next page), which are part of the structural fabric of the TVZ. The major fault in the immediate area of Lake Okaro is the Ngapouri Fault, a northeast striking normal fault dipping to the northwest, which outcrops to the southwest and east of the lake (Lloyd, 1959). Lloyd (1959) noted a line of hydrothermal eruption craters following the trace of the Ngapouri Fault, while Hedenquist & Henley (1985) noted that the eruption craters all occur on the hanging wall of the fault, with Lakes Ngahewa and Okaro occurring off the trace (by ~ 500 metres). It has been hypothesised (Nairn et al., 2004) that the Rotomahana Fault (to the east of Okaro) is an extension of the Ngapouri Fault; while this is possible, an unnamed fault (Nairn, 2002) accompanied by a number of hydrothermal eruptive craters occurs along strike of the Ngapouri Fault roughly 500 metres north of the Rotomahana Fault - this is the structure that Lloyd (1959) identified as the Ngapouri Fault and is much more likely to be its continuation. This is the interpretation illustrated in Figure 2.



2.1.1 Sedimentary Response in Volcanic Settings

The erosion response on hillsides to the deposition of volcanic material is an important issue for regional planners, as the rapid influx of sediment to waterways may result in the filling of those waterways and subsequent flooding of surrounding land or damming of smaller tributaries, as happened after the AD1991 Mount Pinatubo eruption (Scott et al, 1996). Studies into erosion after the 1980 eruption of Mount St Helens, USA (Collins & Dunne, 1986), showed that there was a very rapid decline in the amount of material being eroded from hillsides, with a drop of one to two orders of magnitude of material being eroded over a 3 year study period. There are 2 main types of immediate post eruption runoff and erosion:

- 1) Rills – centimetre- to decimetre-scale erosion channels cut by water running down a slope. Once formed, rills are preferential water migration pathways because they

provide an already made conduit. Rills are the same features as gullies, except gullies are on a metre-scale;

- 2) Sheetwash – unconfined slope runoff with no preferential pathways being formed.

Collins and Dunne (1986) found that sheetwash was the dominant erosive process on areas where the tephra was covering knocked-down vegetation, being 66% to 92% more abundant on cleared hillsides of the same gradient. They also found that rill networks developed around microtopography (formed by tree roots, boulders, etc), and that the majority of rills stopped forming when they reached more-consolidated materials at the base of the tephra deposit. The first 10 months after the eruption showed the greatest amount of rill development, with the largest rills becoming small gullies. The depth of the tephra in this area affected rill and gully formation, with rill formation halting when the fresh, unconsolidated tephra was eroded from the underlying soil (which was highly permeable with a dense root mat that helped reinforce the soil surface). Rill density was initially very high (up to 5 per square metre), but as the rills grew larger they coalesced and the density decreased. Rills with small cross-sectional areas (less than 32 cm²) were obliterated within 3 years through processes such as aggradation in rills over permeable layers, or by destruction of the inter-rills making the rills larger. Similar findings were made at Paricutin, Mexico (Segerstrom, 1950), although more information was gathered about the formation of erosion features in that study. Scott et al (1996) found in the aftermath of the 1991 eruption of Mount Pinatubo that rill formation began almost immediately after tephra deposition, and quickly cut through the tephra and into the pre-existing ground surface.

It is known that the erosion response to the AD1886 Tarawera eruption was rapid, and that large-scale rill formation took place within weeks to months (Keam, 1988); little is known about the termination of rill formation. Hillsides to the north of Lake Okaro are covered in rills, and the depth of the rills appears commensurate with the thickness of the Rotomahana Mud in that area, thus this aspect of the study is to determine at what depth(s) of incision, and how long after deposition, rill formation stopped.

2.1.2 Hydrothermal Eruptions

Hydrothermal eruptions are common events in many geothermal areas (Brown & Lawless, 2001), and prehistoric eruptions are inferred to have occurred in many geothermal fields in New Zealand. Products of two large (10⁶-10⁷m³ total erupted volume) eruptions have been identified in the Kawerau geothermal field in the northern

TVZ, emplaced at 14,500 and 9,000 years before present (BP) (Nairn & Wiradiradja, 1980). Possibly the largest in New Zealand occurred some time between 20,000 and 3,700 years BP at Rotokawa near Wairakei in the lower TVZ, with a single event ejecting material over 13 km², with 3 metre diameter blocks being thrown out of the crater (Collar & Browne, 1985). Around 20 years after the AD1886 Tarawera eruption, between 1900 and 1904, the Waimangu area, which had no geothermal activity prior to the eruption, was host to the “Waimangu Geyser”: a cyclic hydrothermal eruption with a recurrence interval of approximately 36 hours (Browne & Lawless, 2001). In 1917 at Waimangu, what was then called Frying Pan Flat underwent a hydrothermal eruption that ejected material up to 800 feet (240 metres) into the air and spread it over many thousands of square metres, killing 2 people (Grange, 1937; Nairn, 2002). Material from Frying Pan Flat can be found on the hills immediately to the north of Lake Okaro in a deposit between 2 and 10 centimetres thick, where it has been locally reworked in erosion structures on the Rotomahana Mud and provides a useful datum in trenches and pits.

2.1.2.1 Hydrothermal Eruption Mechanisms

Hydrothermal eruptions have been said to differ from phreatic and phreatomagmatic (steam-driven eruptions with juvenile igneous material present) eruptions, in that phreatic eruptions involve direct magmatic heat input, whereas hydrothermal eruptions do not have direct relationship to newly introduced magma, instead relying on hydrothermal systems to provide eruptive energy (Nairn & Wiradiradja, 1980). Browne & Lawless (2001) draw a distinction between phreatic and hydrothermal eruptions based on the nature of the water the magma interacts with, considering an eruption phreatic (or phreatomagmatic) if the water is cold, and hydrothermal if the water is part of a convecting hot water or steam-dominated hydrothermal system; hydrothermal eruptions are then broken down into hydrothermal and magmatic-hydrothermal (where the hydrothermal eruption is triggered by magmatic input either directly by the magma or indirectly through magma degassing or heat flux). Volcanologists do not find these subdivisions workable, and instead favour the view that an eruption is hydrothermal if and only if it involves a hydrothermal system, and phreatic (or phreatomagmatic) if there is magmatic or volcanic input into the system prior to eruption (Mastin, 1991). For the purposes of this report, an eruption is termed hydrothermal if there is evidence that the eruption disturbed a hydrothermal system, in which case hydrothermal alteration of ejecta

would be expected; otherwise the eruption is phreatic or phreatomagmatic (after Mastin, 1991).

Browne & Lawless (2001) provide 5 models to account for the development of hydrothermal eruptions.

- 1) A simple “cap-rock rupture” eruption results if fluid pressures exceed lithostatic pressure and the tensile strength of a field-wide cap-rock, resulting in a single eruption releasing and equalising the pressure (potentially an initiation mechanism, but it would result in a single non-sustained eruption (eg, the phreatic eruption of La Soufriere de Guadeloupe in 1976; Browne & Lawless, 2001), which is not like the majority of observed hydrothermal eruptions).
- 2) An eruption may also follow accumulation of vapour in the near surface because of a decrease in volume of the hydrothermal reservoir, which increases the depth at which boiling takes place (this is thought to be the mechanism of hydrothermal eruptions in over-exploited geothermal fields. Bixley & Browne, 1988). This suggests that a drop in the hydrothermal reservoir, and hence in the hydrothermal water table (not including input of fresh, cold, meteoric water input which would depress the hydrothermal water table but allow the steam to cool and dissipate), would lead to the water boiling point occurring deeper, and hence more steam could accumulate below the surface. Once lithostatic pressure was exceeded by vapour pressure the eruption could occur (this could be provided by a drop in atmospheric pressure after droughts or long periods with little rain; Bixley & Browne, 1988).
- 3) Pressure release at depth from hydraulic fracturing, local tectonic dilatancy, decrease in overburden, or lowering of water table is thought to have caused a large number of eruptions in Yellowstone, USA, 24 hours after a large earthquake in 1959; Browne & Lawless, 2001).
- 4) Addition of magmatic heat or gas (magmatic-hydrothermal) can cause the pressure to increase faster than the system can release it, resulting in explosive disruption and release. (Note: This would be the exact same as a phreatic eruption unless juvenile volcanic materials were present, in which case it would be phreatomagmatic.)
- 5) Progressive flashing drives eruptions that start near-surface, with steam lifting material off the ground and thus lowering the overburden on the rest of the system. This results in a progressive eruption that digs itself deeper with time

until pressure is equalised, and is thought to be the mechanism by which the majority of hydrothermal eruptions proceed.

Examples of eruption by each of these mechanisms can be found, and it is entirely possible more than one of the mechanisms may operate during any given eruption.

2.1.2.2 Previous Work at Lake Okaro

The distribution of material from Lake Okaro was mapped by Cross (1963) during a study of soils forming in hydrothermal eruption deposits; he found material out to a distance of approximately 65 chains (1300 metres) with a maximum depth of just over 40 feet (12 metres), giving an approximate ejecta volume of 4,800,000 yards³ ($3.67 \times 10^6 \text{ m}^3$). Cross also found that the Okaro-Breccia was directly deposited on top of ash from the Kaharoa eruptive episode of approximately 700 years ago, with Nairn et al. (2004) determining that the ash was from a late stage within the eruption (the late stage being dated at approximately AD1314 \pm 12 years through “wigggle-matching” of ¹⁴C dendrochronological ages from samples proximal to the Kaharoa vents on Mount Tarawera).

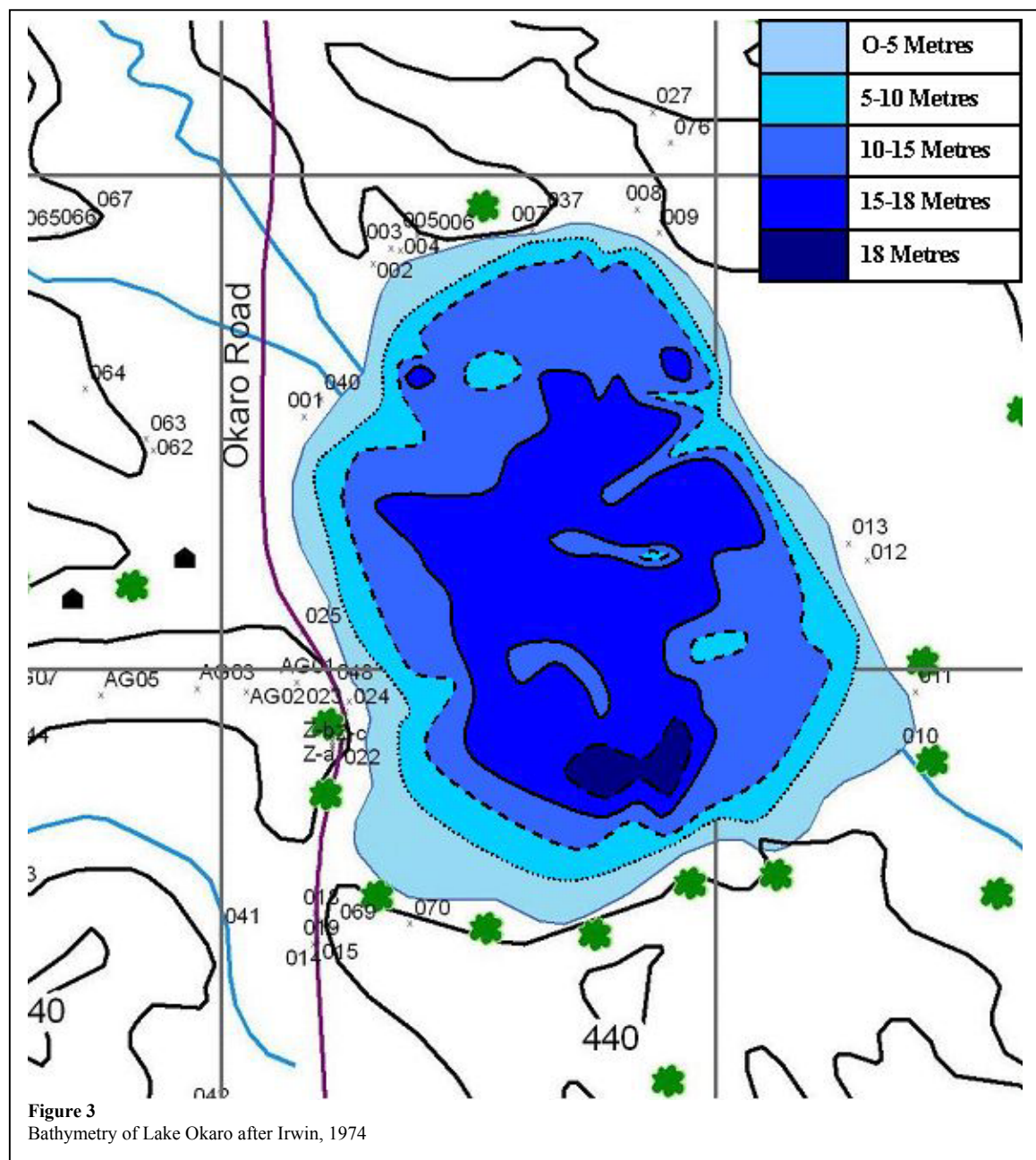
Bathymetry of Lake Okaro (Figure 3) was determined in 1974 (Irwin, 1974), with the deepest part of Lake Okaro identified as being toward the south end of the lake where the tallest cliffs are. A pair of anomalous 15+ metre-deep points occur in the northwest and northeast of the lake where the depth grades from 10 to 15 metres. These are each oval features with dimensions of approximately 15x30 metres, and relatively close to the shore; the eastern one is associated with cliffs at the lake margin. The lake generally averages 15 metres deep in the central area, although there are 3 ridges, one of which rises more than 5 metres higher than the floor. The southeast corner shallows from the centre to the shore where the outlet stream is, while the deepest part, 18 metres, is at the southern end of the lake (where the cliffs are at their steepest). The 18-metre contour covers an area roughly 150 metres east to west by 50 metres north to south. The lake averages 12 metres depth, giving an estimated volume of $5.76 \times 10^6 \text{ m}^3$.

At first glance, the estimated volume of ejected material in the Okaro Breccia, $3.67 \times 10^6 \text{ m}^3$, could easily be accounted for given the estimated volume of the lake ($5.76 \times 10^6 \text{ m}^3$). Although the volume of the Okaro Breccia can be accounted for in the volume of the lake, the presence of a cliff of Okaro Breccia on the eastern shore of the lake suggests that the lake likely formed after the local drainage was dammed by the deposition of the breccia. Hedenquist & Henley (1985) determined that the volume of observed ejecta

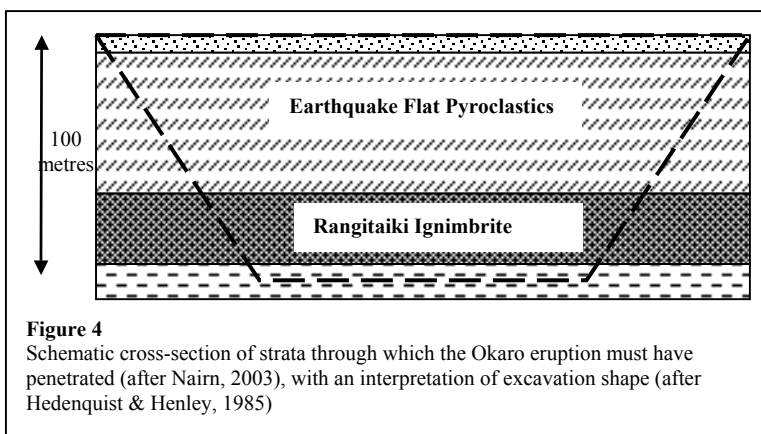
Lake Okaro: Explosions and Erosion

could be fill a crater 250 metres in diameter with a focal depth of less than 100 metres (Figure 4, next page) and “a shape midway between a cone and a cylinder” (Hedenquist & Henley, 1985).

With a focal depth of less than 100 metres the majority of the material ejected would be Earthquake Flat Pyroclastics and Rangitaiki Ignimbrite; the Rangitaiki Ignimbrite is welded, so it likely has a relatively high material strength (uniaxial compressive strengths between 15 MPa and 23 MPa have been experimentally determined for welded tuffs (Quane & Russell, 2003); this is low compared to granites and basalts, but would high relative to other units in the area), while the Earthquake Flat Pyroclastics, being unconsolidated, should be much weaker and would be expected to slump more readily.



Since the topography in the area is controlled by Earthquake Flat Pyroclastics (Nairn, 2002), present day hills with no evidence of slope failure could be used as proxies for slope angles that the



Earthquake Flat Pyroclastics can withstand without slumping. If the land had been perfectly flat prior to eruption, and if the current lake basin is largely the result of slumping into a crater (i.e., if the centre of the lake was the deepest part and external sedimentation played little part in the infilling of the crater, then the slopes would have had to slump to approximately 5° to reach present bathymetry), then it could be expected that the slumping would have had to occur on angles much less than that of the present hillsides in order to form the lake at its present size. Since the hills show no evidence of failure to such a low angle, it seems unlikely that slumping at the margins of a single crater could form the present lake.

Nairn et al. (2004) suggest that the Okaro eruption was initiated by intrusion and arrest of a basaltic dyke at depth along the Ngapouri Fault. They cite increased $\delta^{13}\text{C}$ proportions in calcite from drill cores in the Waiotapu geothermal field (the location of the Waiotapu geothermal field is given in Figure 2) as being evidence for a pulse of CO_2 approximately 10 times greater than current emissions. In addition, the lubrication effect of rising fluids and gases could help explain displacement along the Ngapouri Fault concurrent to the hydrothermal eruptions along it. They do acknowledge that the timing of the CO_2 pulse “cannot be precisely defined”, but, coupled with the determination that the Kaharoa eruptions were initiated by basaltic intrusion (Leonard et al, 2002), the circumstantial evidence leads them to the conclusion that a basaltic dyke could have been intruded into or along the Ngapouri Fault and could thus have primed the Waiotapu geothermal system for hydrothermal eruption.

2.2 Methodology and Fieldwork

Fieldwork was carried out in January and June 2005. Collected samples were bagged and labelled in the field before being sent back to Dunedin. An outcrop and sample list can be found in Appendix C. Outcrop coordinates were determined using a Garmin etrex

Venture hand-held GPS unit, and were converted to New Zealand Transverse Mercator units based on the GD2000 projection using ArcGIS 9.0; no differential correction has been made on the GPS data, so an accuracy of ± 15 metres should be assumed. Both New Zealand Map Grid and Transverse Mercator coordinates are available in the Excel file “Okaro Sample Data” on the accompanying CD-ROM.

All location maps were compiled in ArcGIS 9.0.

2.2.1 GPS Mapping and Rill Analysis

The rills were mapped using two Trimble GeoXT hand units, with one being set up as a base station and the other as a rover to gather the location data. Differential correction between the two units was made using Trimble Pathfinder Office v3.001, and the resulting data was input into ArcGIS 9.0 with Vertical Mapper software. The error associated with the GPS data points was typically ± 0.5 metres vertical and ± 0.2 metres horizontal.

Rill analysis was carried out using a 1-metre hand auger and tape measure. Holes were drilled cautiously and the hand auger was checked regularly to see when the base of the Rotomahana Mud was reached. The tape measure was then extended down the hole, with the depth to the base of the hole being measured from ground level. All depth measurements should be assumed to have a margin of error of ± 5 cm. The maximum depth that could be drilled was 0.95 metres on flat ground – when on a slope this was reduced to 0.9 metres before the auger could no longer be turned.

Auger locations and hole data can be found in Appendix D

2.2.2 Grainsize Analysis

Samples for grainsize analysis were transported to the Institute of Geological and Nuclear Sciences Wairakei Research Centre, where they were dried at 55°C before being dry-sieved to remove particles coarser than 1λ . Hedenquist & Henley (1985) found no evidence for clays in X-ray diffraction analysis of samples from the Okaro Breccia, so aggregation could be kept to a minimum. In order to prevent coarse particles clogging the sieve for finer particles, the samples were put through -1λ sieves prior to the 1λ sieves. Grainsize analysis using between 0.5 grams and 1.5 grams of the finer than 1λ fraction was made using a Coulter LS130 particle size analyser; quantity necessary for analysis was variable, with some samples needing a detergent deflocculant in order for the material to mix properly. All remaining material was transported back to Dunedin where it was sieved by hand from -4λ to 4λ . Because the samples were not wet-sieved prior to

drying, aggregates were unavoidable; where practical (size fractions larger than -1λ) aggregates were disassociated by hand or rolling pin between 2 sheets of paper, otherwise gentle rubbing of the bulk grains was used to disassociate weaker grains against stronger grains – some primary clay-like aggregates (-0.5λ to 0λ) were destroyed in the process, although this was uncommon and would account for at most 0.1 grams per sample. Additional weight-loss was noted between Wairakei and Dunedin, possibly through incomplete drying at Wairakei (potential with samples OU75041-OU75046 and OU75057-OU75066 as these samples were dried for less than 12 hours); where practical, these weights were recalculated prior to sieving in Dunedin. Amounts of material collected for grainsize analysis were variable due to outcrop conditions, with the average being approximately 200 grams (complete weight and analysis data can be found in Appendix E).

The Coulter grainsize data was generated in volume percentages while the sieve data was generated in weight percentages. In order to be able to compare the two data sets, the volume percentages were recalculated to weight percentages so that the two data sets could be merged. The following formula was used (after Glicken, 1996):

$$W_f = \frac{100 \psi_f V_f}{\psi_f V_{fi} + 2 \psi_c (100 - 4 V_{ct})}$$

Where:

W_f = weight percent of size class finer than 2λ

V_f = volume percent of size class finer than 2λ

V_{fi} = total volume percent of all size classes finer than 2λ

ψ_c = density of material coarser than 2λ

ψ_f = density of material finer than 2λ

Due to the nature of the material used, which is rhyolitic and quartz-rich, the density used for both the coarse and the fine fractions was that for quartz in samples OU75041 to OU75046 (2.62 g/cm^3), and that for cristobalite (2.27 g/cm^3) in samples OU75047 to OU75066, which have a noticeable population of opal as well as quartz evident in thin section. An alternate method of combining the two data sets is that of Segschneider (2000), whereby the finer than 4λ (pan) fraction was ignored if it was less than 5% by weight or, if over 5% by weight, the coarser than 4λ fraction was cumulated to 100% minus the pan fraction and then projected to 100% using the coulter data; this method,

however, exaggerates the weight of fine material in the sample when the volume percent is included and thus was not used.

A matrix sample of Earthquake Flat Pyroclastics (OU75067) was later hand-sieved using a similar method to that employed for the Okaro-Breccia matrix samples, except that no Coulter analysis was made of it. This sample was split to 3/8 of the original sample (~200 grams) before being dried at 60°C for 24 hours. It was not wet sieved prior to drying, and was hand-sieved to 4.5 λ .

Analysis of grain size data was carried out in two ways. The first was the plotting of histograms, and frequency and cumulative frequency graphs using Microsoft Excel 2000; the second way was using KWare SFT software v.2.19.0162. The KWare SFT software was used for plotting cumulative probability graphs and Folk graphical statistics.

2.2.3 X-Ray Diffraction

Material from the pan-fraction after sieving for samples OU75042 to OU75066 was ground down to a fine powder and run through a PANalytical X'Pert-Pro MPD PW3040/60 XRD with a Rapid RTMS X'Celerator Detector for a preliminary clay analysis. The resulting XRD traces were analysed using PANalytical X'Pert HighScore software, which provides a 'best-fit' mineral assignment to the resulting peaks. The 'best-fit' was then refined by assessing the highest probability minerals with the known mineralogy of the samples based on binocular microscope and thin section analysis. The resulting assemblages are presented in Appendix F.

2.2.4 Cathodoluminescence and Electron Microprobe Analysis

Cathodoluminescence was carried out on the JEOL JXA-8600 electron microprobe analyser, with cathodoluminescence attachment, at Otago University. Quartz grains picked for cathodoluminescence were chosen from the 2 λ fraction of samples OU75044 and OU75068 (crushed up Earthquake Flats pumice); these were mounted onto double-sided tape to enable them to be kept in position prior to being made into a polished section. Picking was done under binocular microscope at 40x magnification, and only grains that showed no sign of cleavage or twinning were chosen; some plagioclase was accidentally collected from the Okaro-Breccia, and was then used to help standardise the microprobe during analysis.

To test whether or not cathodoluminescence would be useful in assessing the provenance of the loose quartz grains in the Okaro-Breccia, a number of quartz grains from a Fiordland granodiorite (OU75175) were also mounted onto the same section.

Investigation by Götze et al (2001) indicates that quartz cathodoluminescence can be used for provenance studies, and this current investigation of the grains showed that the cathodoluminescence characteristics of plutonic quartz were vastly different to that of volcanic quartz, supporting the findings of Götze et al (2001).

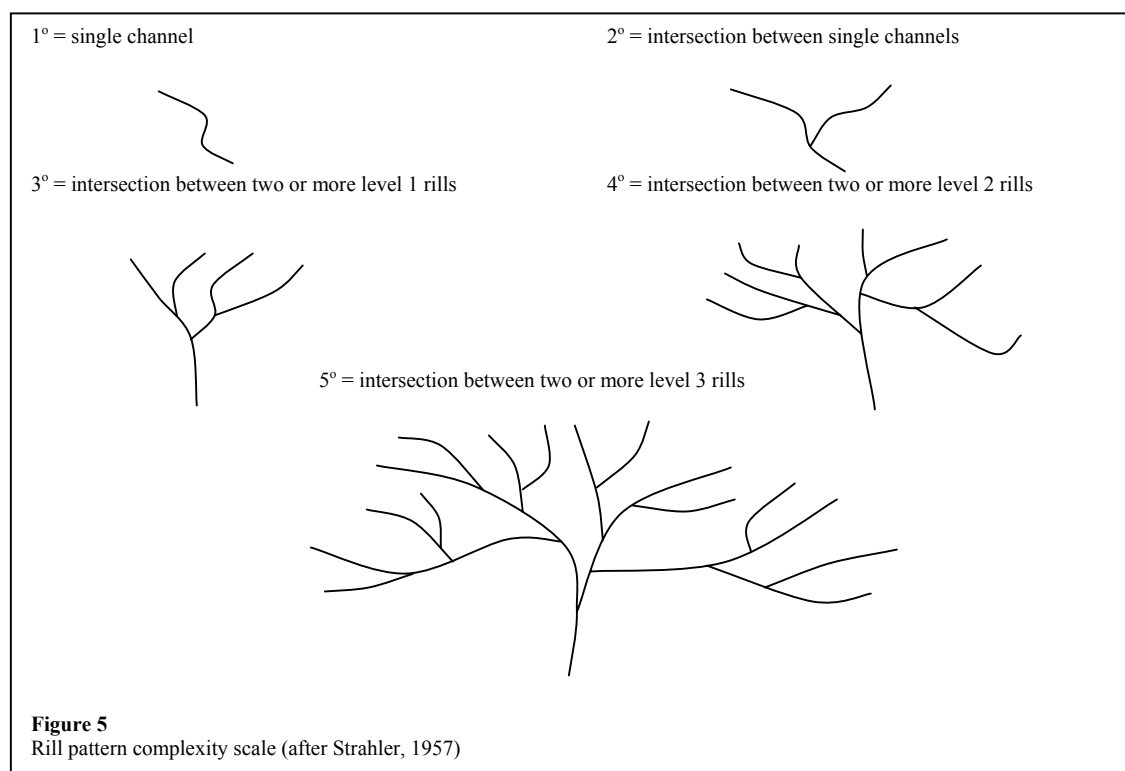
Inspection under cathodoluminescence of the quartz grains from the Earthquake Flats pumice and the Okaro-Breccia showed that some quartz grains have attached glass. Glass was distinguished from plagioclase, which also showed no cathodoluminescence, by EDS before being probed for major element composition by Lorraine Paterson. Plagioclase in the Okaro-Breccia sample was used for standardising the analyses. Major element data can be found in Appendix G. Full cathodoluminescence images can be viewed on the accompanying CD-ROM.

3 Erosion Rills North of Lake Okaro

The rills on the hills to the north of Lake Okaro vary in depth dependent on their location relative to the slope. At the top of the hills they are not noticeable beneath the grass until they have attained a depth of approximately 5 centimetres, although at the base of the hills they can be a metre or more in depth. Depth increases down-slope, whereas complexity decreases down-slope (which is to say that there are many small rills at the top of the slope, and few larger rills toward the base of the slope).

3.1.1 GPS Mapping of Rills

GPS mapping of two adjacent valleys (location indicated on base map in Appendix B) showed minor differences between rill structures within the different valleys. Drainage patterns were ranked on a scale based on the number of connections between rills (Figure 5, after Strahler, 1957), with a single channel being having a primary (1°) complexity; an intersection between two 1° channels results in a rill with a secondary (2°) complexity, an intersection between 2° channels forms a tertiary (3°) complexity, and so forth. The complexity scale only increases when it involves intersections between rills with the same complexity, so a 1° and a 2° result in a 2° , while a 2° and a 2° result in a 3° .



Lake Okaro: Explosions and Erosion

Both valleys exhibited similar drainage patterns (Figures 6 and 7), with the valley walls having exceptionally simple rill structures with occasional connections; the heads of the valleys, on the other hand, showed a larger degree of complexity. Interconnections between rills in the west valley reached 4° complexity at the head of the valley, while the



Figure 6
Panorama of valleys where rill erosion was studied

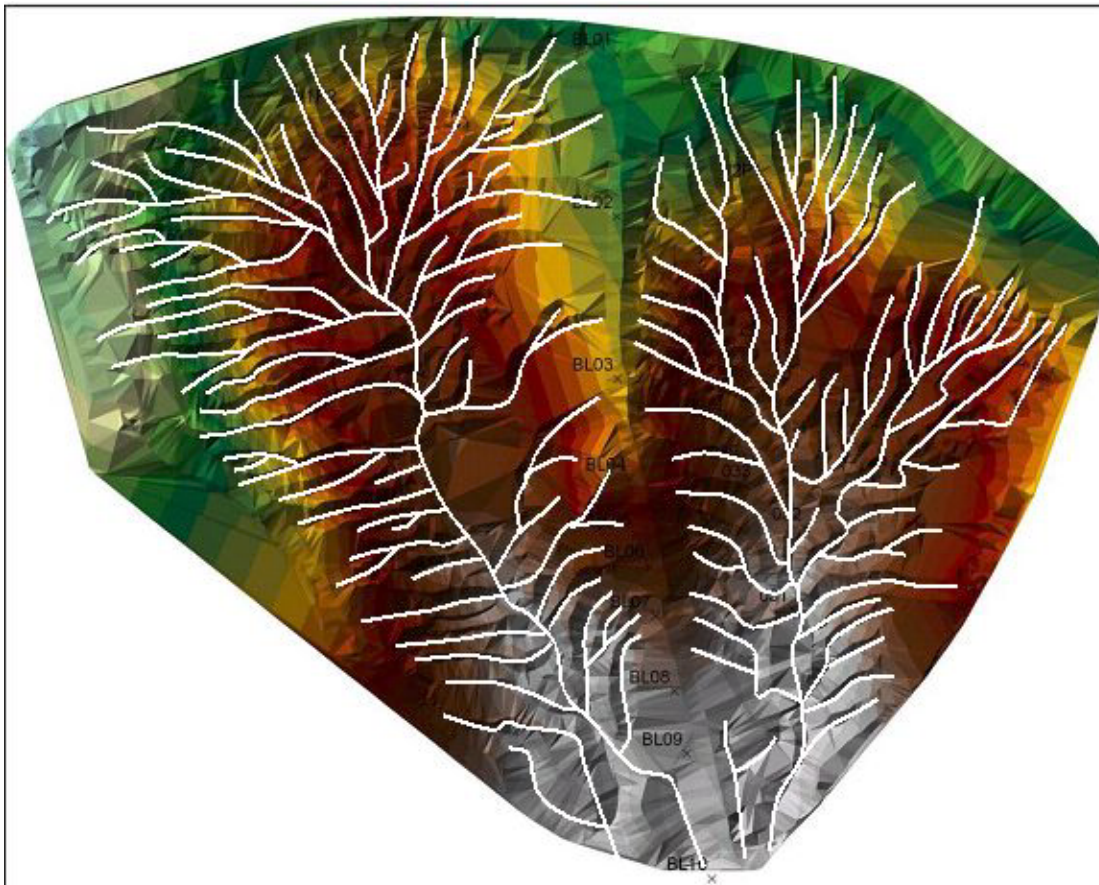


Figure 7
Rill complexity mapped out on a triangular irregular network (TIN) created from GPS elevation data (colour intervals represent 1 metre elevation changes)

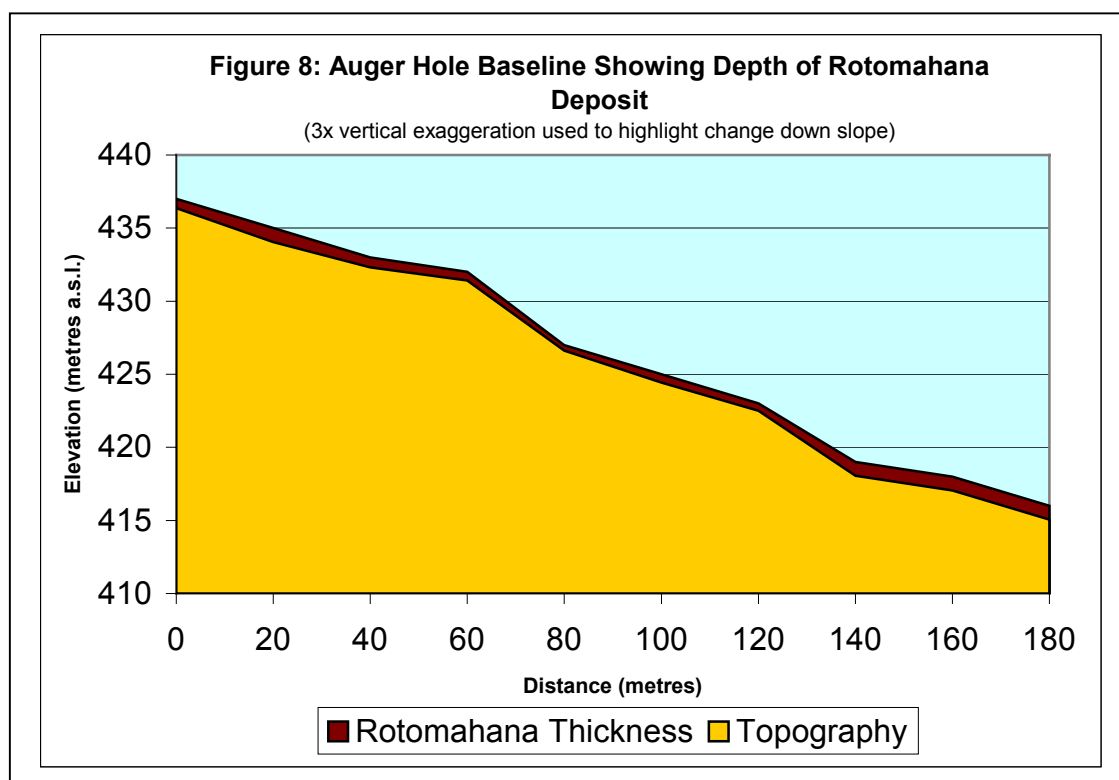
east valley, which had two smaller heads each of 3° complexity, did not reach 4° complexity until the two heads combined.

3.1.2 Rill Depth

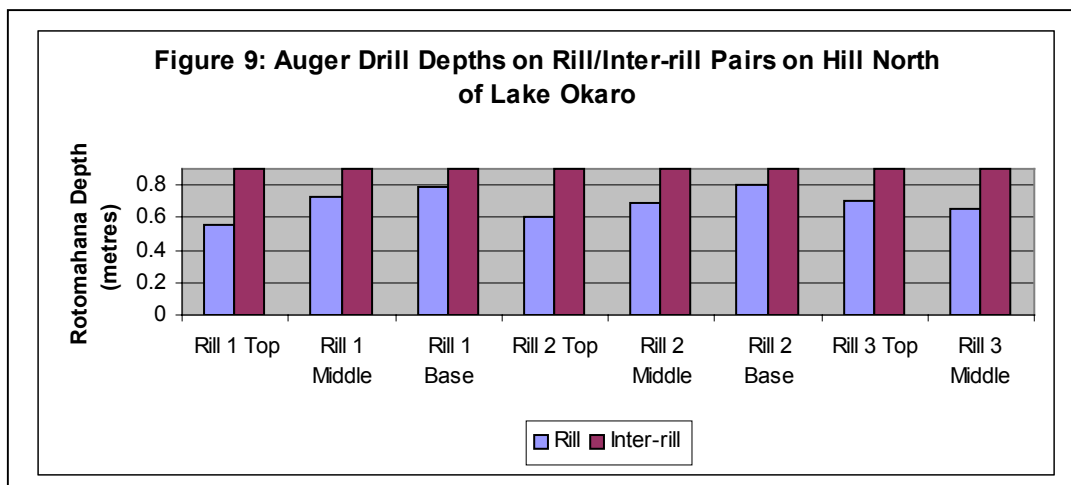
A baseline along the ridgeline travelling south into the valley at 1896800mE, 5756350mN showed a roughly uniform veneer of Rotomahana Mud along the crest of the ridge, which thinned at the top of the slope before thickening down-slope (Figure 8). On top of the ridge the Rotomahana Mud had a ‘muddy’ feel, while toward the bottom of the slope it was divided into a sandier upper layer and a muddier lower layer¹.

Rill depth varies down-slope, with the rills being shallowest at the top of the slope and deepest toward the base. Rotomahana Mud on inter-rill ridges is consistently thicker than the hand auger could penetrate (>0.90 metres). The depth to the base of the Rotomahana Mud in the rills is between 0.55 metres and 0.80 metres (Figure 9, next page). Rill depth set 3 showed a reversal from the previously observed trend due to a change in slope gradient.

A 1.64 metre deep pit was dug in the floor of the valley (Figure 10), and revealed that there was a buried channel that cut 0.31 metres below the AD1886 soil horizon. The channel has been filled with what is apparently fines-depleted Rotomahana Mud. The age



¹ These are qualitative descriptions based upon the feel of the material between fingers and do not assign specific grain sizes to the deposit.



of formation for this channel cannot be determined with any accuracy other than post-AD1886 eruption, but the presence of a 0.07 metre thick sub-horizontal layer of hydrothermal eruption breccia related to the AD1917 Frying Pan Flat hydrothermal eruption crossing the channel approximately 0.10 metres above the AD1886 soil horizon provides a good marker for the length of time it took for the channel and valley floor to refill after erosion.

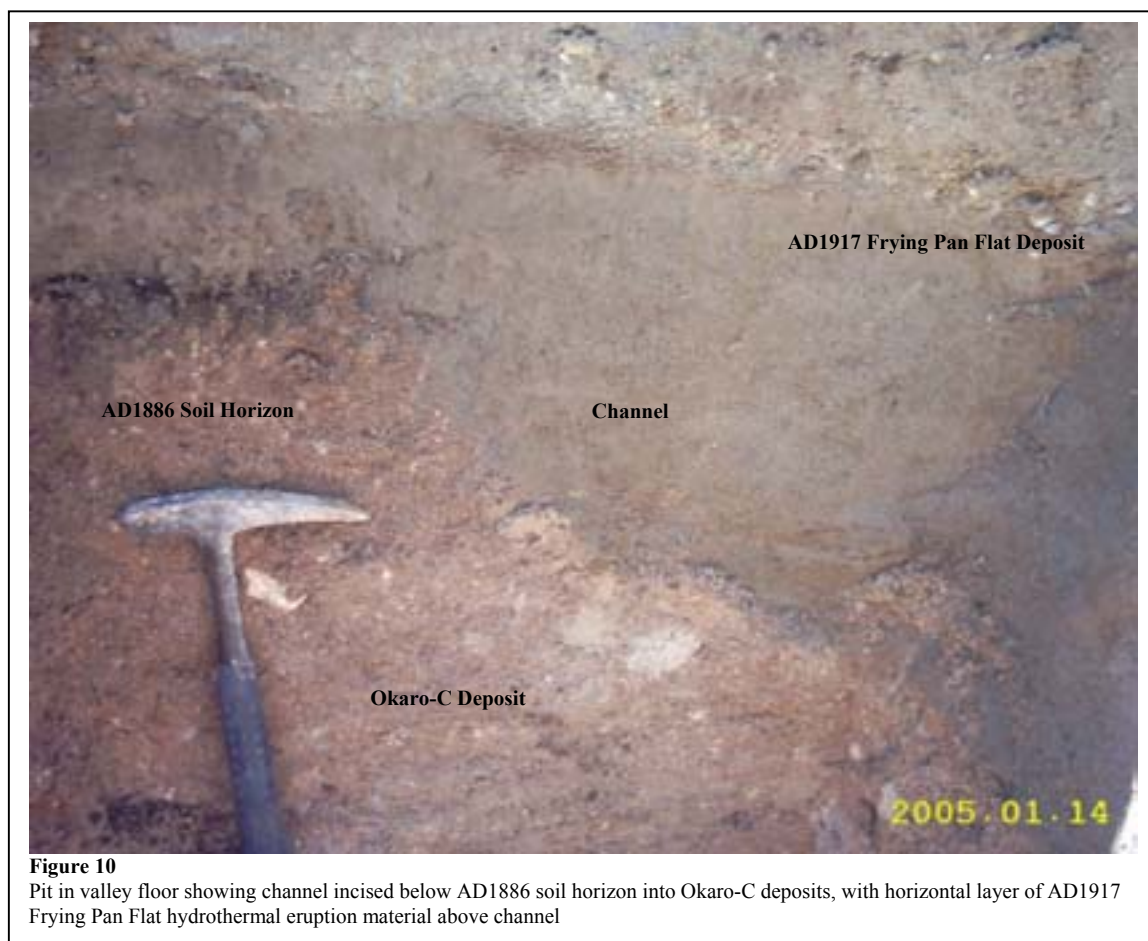


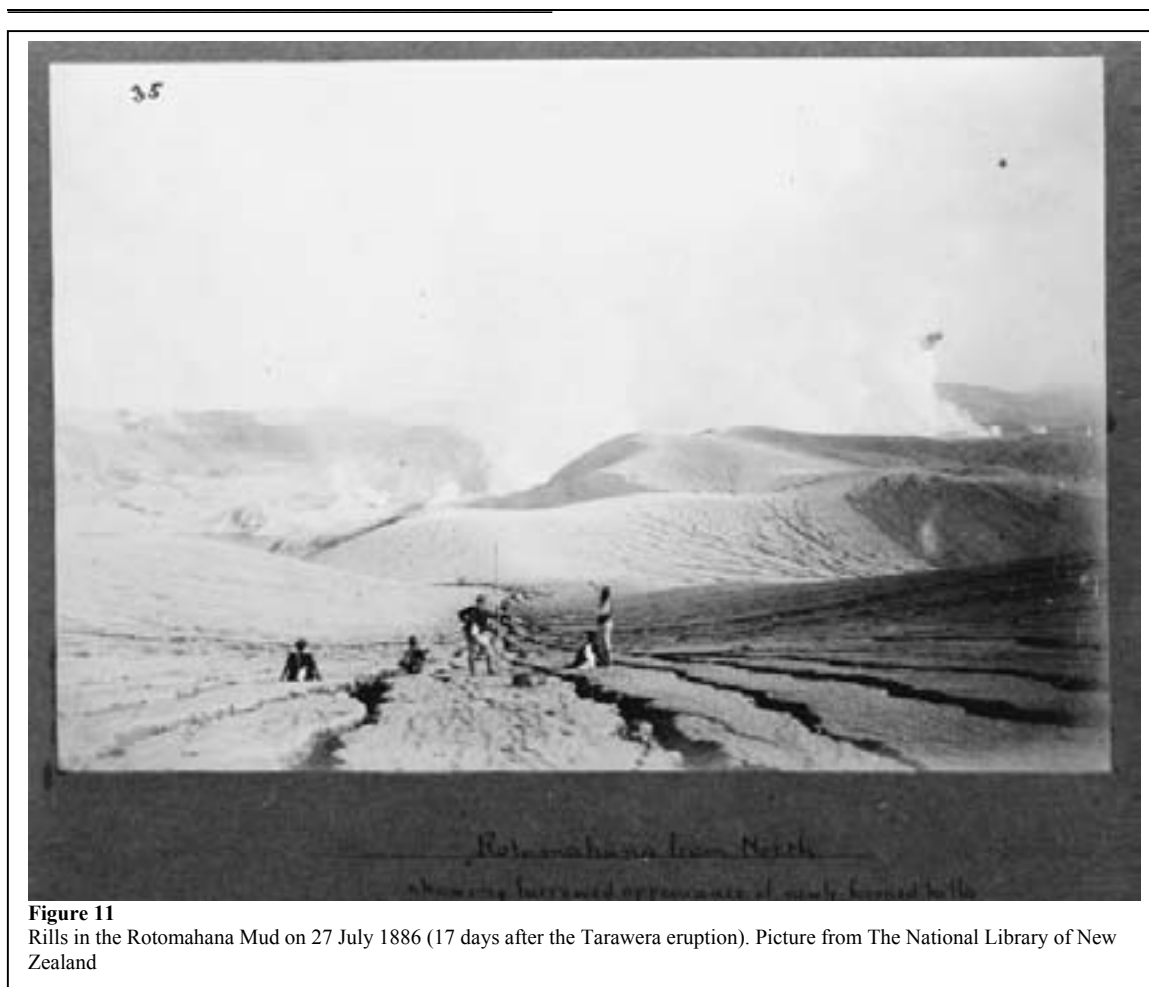
Figure 10
Pit in valley floor showing channel incised below AD1886 soil horizon into Okaro-C deposits, with horizontal layer of AD1917 Frying Pan Flat hydrothermal eruption material above channel

3.1.3 Interpretation and Discussion

The complexity of the drainage pattern worked out to be the same for each valley, including for the two smaller catchment heads that make up the east valley, leading to a hypothesis that the complexity of the drainage systems examined depends entirely on the catchment size. In the east valley the smaller catchments are each of similar size and formed the same complexity (3°), while both the east and west valleys in total are similar size and formed the same complexity (4°). Strahler (1957) found that the complexity of the drainage pattern was related to the area of the catchment as well as to the material making up the catchment; materials with similar properties developed similar complexity drainage, while materials with different properties developed different drainage complexities.

Since the auger holes failed to penetrate the Rotomahana Mud on the inter-rill ridges and succeeded within the rills, it can be concluded that the rills have formed entirely within the Rotomahana Mud and represent the immediate sedimentary response to the AD1886 eruption. Historical evidence (Keam, 1988) suggests that rill formation occurred over a matter of weeks to months after the eruption (Figure 11, next page), but while the majority of erosion must have stopped at that time (because there was little subsequent modification of the rill system), minor erosion was still proceeding well into the 1900s (Grange, 1937). The cessation of rill formation in the Rotomahana Mud seems to follow a similar pattern as erosion cessation on the volcano 'Vulcan' in Papua New Guinea (Ollier & Brown, 1971), whereby major gully formation occurred within the first 5 years after the 1937 eruption and then stabilised; Ollier & Brown (1971) did not find any evidence for why erosion slowed, but it was before vegetation reclaimed the slopes.

Erosion into the soil below freshly deposited tephra was documented occurring after the AD1991 Mount Pinatubo eruption (Scott et al, 1996), but not after the AD1980 Mount St Helens eruption (Collins & Dunne, 1986). In the case of Mount St Helens, rill erosion terminated at the base of the tephra due to the high permeability of the soil horizon (Collins & Dunne, 1986). With Mount Pinatubo, however, erosion into the substrate was put down to large volumes of sand-sized material being transported in fast developing structures (head-cutting at rates of up to 10 metres per hour) scouring the soil in hyperconcentrated flows (Scott et al, 1996); it is not documented if the soil at Mount Pinatubo had high permeability or not, although the soils in the area of Mount Pinatubo are more clay rich and are thus likely to be less permeable than the soils examined by Collins and Dunne (1986) at Mount St Helens (James White, personal communications



2005). If these observations are consistent with other volcanic areas, then high permeability could be the key to the retardation of erosion. In studies into the effects of wildfires on erosion (Prossler & Williams, 1998), it was found that highly permeable soils had lower rates of erosion, due to low overland flow, while low permeability soils had greater rates of erosion, due to greater surface runoff. This suggests that soil permeability is the controlling factor in the cessation of erosion.

The AD1886 soil horizon at Okaro was developed on the Okaro-Breccia, which is poorly sorted and has a relatively high content of fine-grained material (average of 31.64% by weight of material finer than 0.5 mm) suggesting that it would have a low permeability (Manville & Wilson, 2004), thus the presence of the filled channel incised below the AD1886 soil horizon in the valley floor suggests that the initial erosion must have scoured the valley floor in a similar fashion as occurred at Mount Pinatubo after the 1991 eruption (Scott et al. 1996). Thus it seems likely that channel incision terminated at the same time as rill erosion ceased since that is when the influx of sediment from the rills would have declined, in which case the channel was filled by 0.31 metres of sediment and the valley floor was built up by 0.10 metres of sediment between late-

Lake Okaro: Explosions and Erosion

1886/early-1887 and April 1917 when the Frying Pan Flat hydrothermal eruption deposited material over it. This leads to a time-averaged aggradation rate in the channel of ~ 0.013 metres/year (0.41 metres of reworked Rotomahana Mud over 30 years). Since the AD1917 Frying Pan Flat hydrothermal eruption, there have only been 0.41 metres of aggradation in the examined valley floor, which equals 0.0047 metres per year aggradation (0.41 metres over 88 years). This is an order of magnitude lower than the early post-eruption value, and a more accurate representation of the long-term aggradation rate, since much of that area has had grass/shrub cover since that time.

4 Lake Okaro Eruptions

4.1 Breccia Description and Analysis

The Okaro eruption deposit appears as a poorly sorted breccia consisting of angular to sub-angular clasts of large lapilli to block sized pumice and welded ignimbrite, supported in a muddy, fine-grained matrix. The Okaro breccia directly overlies ash from the 0.7 ka Kaharoa eruptive episode, which, in turn is separated by a paleosol from the 1.8 ka Taupo air-fall pumice-lapilli. Overlying the Okaro breccia in most localities is a thin paleosol covered by the Rotomahana Mud from the 1886 Tarawera eruption – where the Rotomahana Mud is absent, the current soil horizon has developed directly on top of the breccia. The breccia can be subdivided into three visually distinct members, Okaro-A, B and C.

4.1.1 Okaro-A

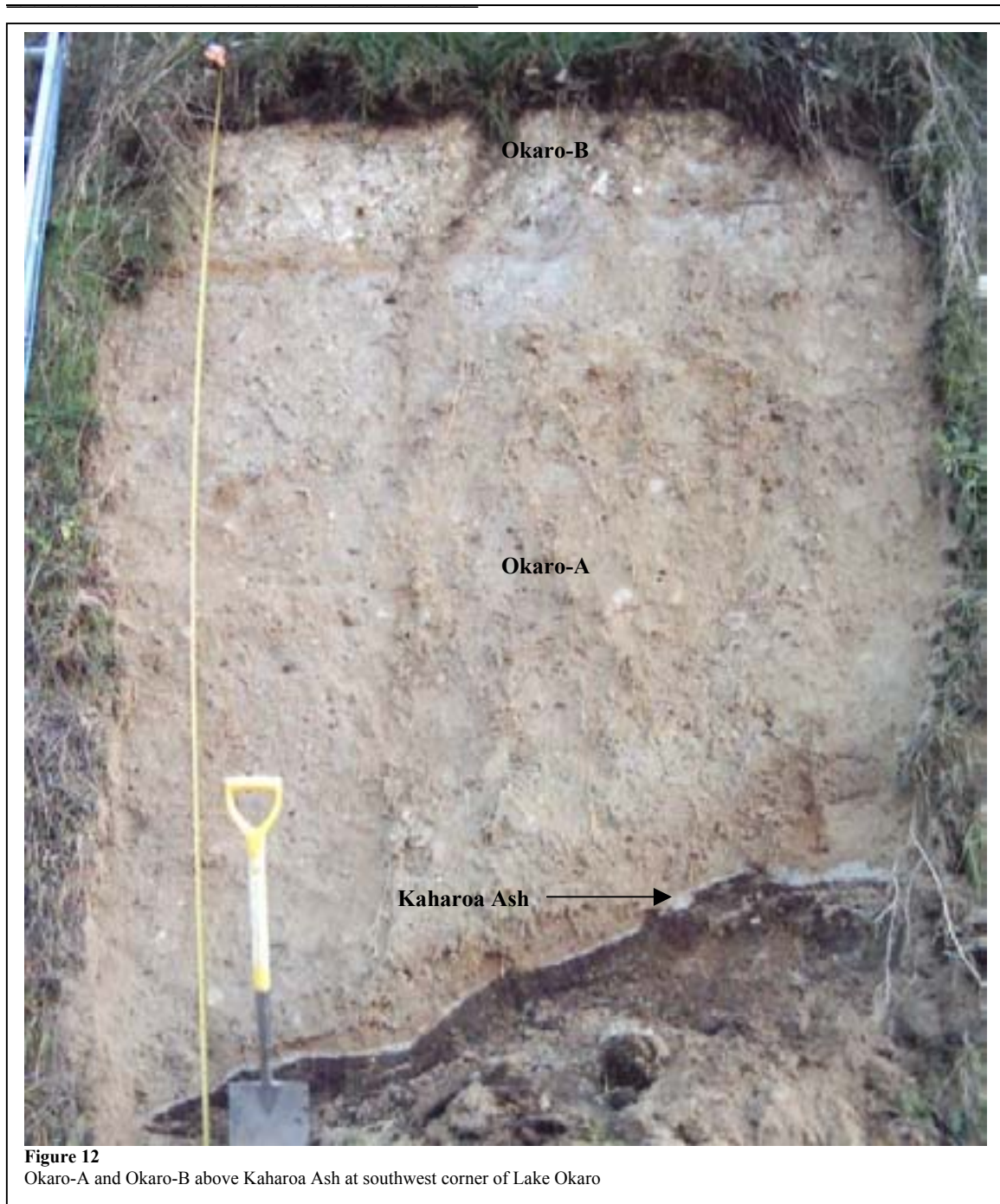
The Okaro-A type locality is the road cut at the southwest edge of Lake Okaro (Grid Reference 1896625mE, 5755425mN). Okaro-A samples, from the measured section (Appendix H), are OU75042-OU75046.

4.1.1.1 Physical Description

Okaro-A (Figure 12, next page) is predominantly fine-grained and matrix supported, with a maximum clast size of 0.10 metres. There are at least 3 visually distinct styles of clast: coarsely vesicular pumice (estimated ~60% of clasts), welded ignimbrite (~35%), and small dark clasts (~5%). Maximum clast size variation is high in section with largest clasts at different levels, varying from 0.40 metres to 0.80 metres in diameter (see measured section in Appendix H), and clast size decreases closer to the contact with Okaro-B.

The matrix consists of coarse ash- to small lapilli-sized fragments, with grains of biotite, quartz and hornblende visible in hand lens; very fine material is also present. Basal bomb-sags are rare. Orange staining defines thin parallel laminae in the lower 50 and upper 100 millimetres; these laminae are not disturbed by either bomb-sags or Okaro-B, and thus are inferred to be post-depositional features.

Okaro-A has a thickness of 2.15 metres at the southwestern edge of Lake Okaro, thinning to 0 metres at a distance of approximately 250 metres from the lake edge; it has not been identified to the north or east of the lake.



4.1.1.2 Petrographic Description

Four thin sections were made from the sieved material from samples OU75043, OU75044, and OU75046, with thin sections from OU75043 and OU75046 being made from the 2λ - 3λ fractions, and thin sections from OU75044 and OU75046 being made from the 1λ - 2λ fractions.

There was not a large amount of variation in the thin sections, with quartz, plagioclase, biotite, clinopyroxene, orthopyroxene, hornblende, glass, and lithic fragments being evident in all of them. The plagioclase exhibits both twinning and common zonation

Lake Okaro: Explosions and Erosion

Table 2
Okaro-A grain size graphical statistics (after Folk, 1980)

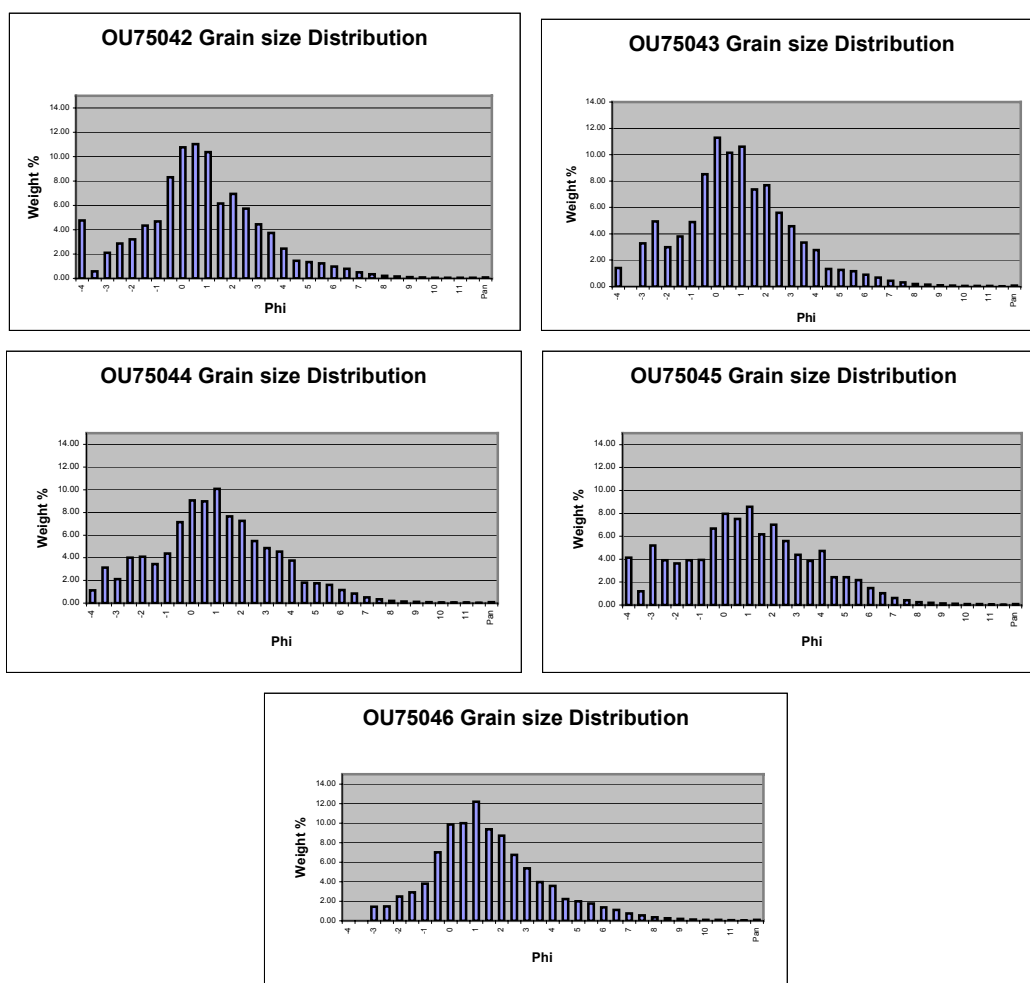
	OU75042	OU75043	OU75044	OU75045	OU75046
Graphic Mean	0.52 λ	0.47 λ	0.66 λ	0.62 λ	1.19 λ
Inclusive Graphic Standard Deviation	2.42 λ	2.22 λ	2.50 λ	2.83 λ	2.17 λ
Inclusive Graphic Skewness	0.05	0.08	0.04	0.03	0.19
Graphic Kurtosis	1.31	1.21	1.13	1.03	1.19

(especially in the coarser fragments), as well as rare cumulate textures in OU75046. Hematite was observed under reflected light as a stain to some lithic fragments in OU75046, as well as being a rare opaque mineral; there is also rare hydrothermal quartz in OU75046.

4.1.1.3 Grainsize Analysis

Raw grain size data can be found in Appendix E. The Okaro-A samples (graphical statistics in Table 2) exhibit similar characteristics, with the exception of OU75046, the uppermost sample from Okaro-A, which showed a finer mean grainsize (Figure 13).

Figure 13
Okaro-A grain size histograms



Graphical statistics (after Folk, 1980) give the Okaro-A deposit an overall mean of 0.57λ , with OU75046 having a mean of 1.19λ . The deposit is very poorly sorted, with an average inclusive graphic standard deviation of 2.43λ (including OU75046; the values ranged between 2.17 (OU75046) and 2.83 (OU75045)), but the deposit, excepting OU75046 (which is fine-skewed at +0.19), has a nearly symmetrical grainsize distribution with an inclusive graphic skewness between +0.03 and +0.08. The Okaro-A deposit is leptokurtic, however there is a trend from OU75042 to OU75045 from leptokurtic to mesokurtic (going progressively from 1.31 to 1.03 before going back up to 1.19 with OU75046).

4.1.1.4 Clay Analysis Using X-Ray Diffraction

XRD analysis (Appendix F) revealed no clays in samples OU75042 to OU75044, with sericite being detected in OU75045.

4.1.1.5 Quartz Origin Using Cathodoluminescence

Under cathodoluminescence the quartz in Okaro-A faintly luminesces against the resin background; this contrast was enhanced once the mount darkened under electron bombardment. The quartz samples from the Okaro-Breccia (Figure 14a, next page) and the Earthquake Flats pumice (Figure 14b, next page) exhibit weak zonation in a similar pattern, whereas a sample of Fiordland granodiorite (Figure 14c, next page) examined as an example of non-volcanic quartz exhibits a distinctive fracture pattern. This textural difference between plutonic and volcanic quartz has been previously described by Götze et al. (2001), and seems to be a reliable method for provenance determination. Due to only having access to one of the potential sources of the Okaro quartz, however, the best that can be said is that the quartz in Okaro-A is volcanic in origin.

4.1.1.6 Glass Electron Microprobe Analysis

Electron microprobe analysis of glass attached to quartz grains from Okaro-A sample OU75044 and Earthquake Flat Pyroclastics sample OU75067 showed very similar major element compositions from the two samples (Table 3, next page). Plotting the glass compositions as CPIW normative values for quartz, orthoclase (including anorthite), and albite on a ternary diagram (Figure 15, page 31) shows clearly that the glasses from Okaro-A and the Earthquake Flat Pyroclastics samples plot close together. (Note that some effects of alkali migration from electron beam intensity (e.g. G6S4), and quartz contamination from a narrow beam burning into quartz below the glass (e.g. G2S3), are evident).

Lake Okaro: Explosions and Erosion

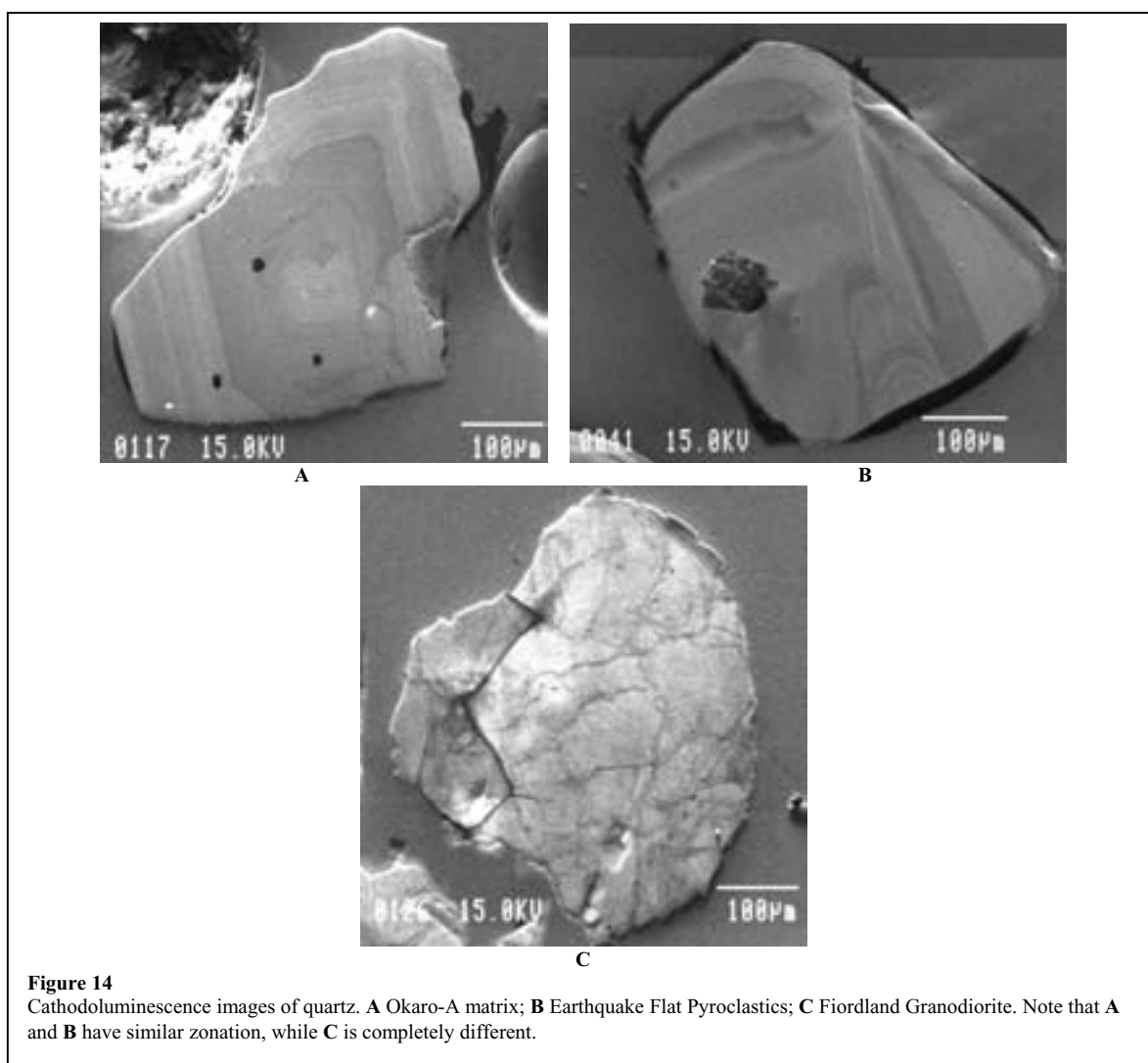


Figure 14
Cathodoluminescence images of quartz. **A** Okaro-A matrix; **B** Earthquake Flat Pyroclastics; **C** Fjordland Granodiorite. Note that **A** and **B** have similar zonation, while **C** is completely different.

Table 3
Electron microprobe-determined oxide values for glass attached to quartz grains

Major element	Earthquake Flat Pyroclastics: OU75067							Okaro-A: OU75044							
	G1S1	G1S3	G2S3	G2S4	G3S1	G3S3	G2S6	G1S1	G1S2	G6S1	G6S3	G3S2	G2S3	G6S4	G6S5
SiO ₂	76.52	76.30	77.48	77.77	78.86	77.11	77.48	77.08	77.41	77.63	77.87	80.35	79.38	80.98	77.87
TiO	0.09	0.09	0.09	0.09	0.09	0.09	0.09	0.06	0.06	0.10	0.09	0.09	0.08	0.09	0.05
Al ₂ O ₃	11.88	12.15	12.05	12.06	12.41	12.36	11.99	12.07	12.00	12.08	12.25	10.11	11.00	12.67	12.30
FeO	0.90	0.80	0.89	0.80	0.90	0.89	0.85	0.85	0.80	0.89	0.76	0.81	0.80	0.85	0.89
MnO	0.03	0.01	0.06	0.06	0.00	0.03	0.05	0.04	0.06	0.01	0.05	0.00	0.03	0.07	0.03
MgO	0.07	0.06	0.08	0.06	0.08	0.08	0.08	0.06	0.05	0.05	0.08	0.08	0.07	0.08	0.07
CaO	0.73	0.72	0.73	0.71	0.73	0.74	0.70	0.72	0.70	0.72	0.75	0.61	0.66	0.71	0.75
Na ₂ O	3.62	3.50	3.43	3.47	3.61	3.38	3.53	3.37	3.45	3.38	3.41	2.77	3.11	1.68	3.04
K ₂ O	4.20	4.26	4.33	4.40	4.22	4.06	4.39	4.31	4.27	4.27	4.28	3.65	3.87	3.53	4.19
Total	98.04	97.89	99.14	99.42	100.90	98.74	99.16	98.56	98.80	99.13	99.54	98.47	99.00	100.66	99.19

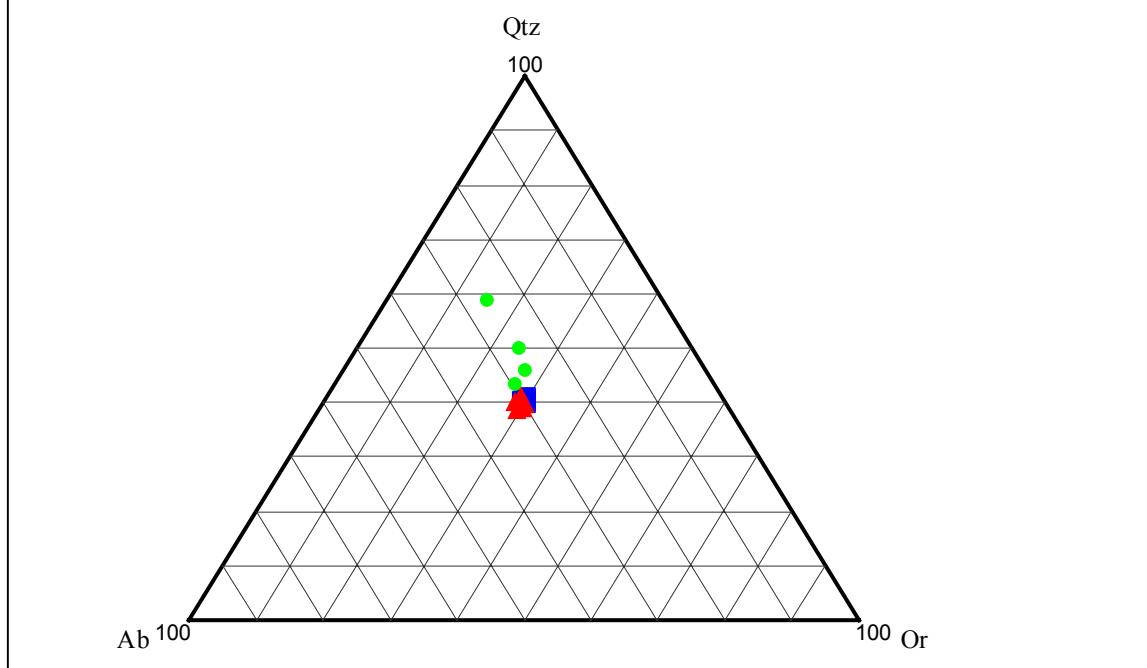
All Fe reported as FeO

Uniformly shaded samples represent analyses suffering quartz contamination and/or alkali migration

Lake Okaro: Explosions and Erosion

Figure 15

Ternary quartz-albite-anorthite diagram plotting glass compositions from the Okaro-A sample OU75044 (blue squares) and Earthquake Flat Pyroclastics sample OU75067 (red triangles). Green diamonds represent samples contaminated by quartz or alkali migration due to electron beam size and intensity in Okaro-A sample OU75044.



4.1.1.7 Interpretation

Okaro-A deposits are only present at the south end of the lake, so it is inferred that the crater that ejected this deposited was also located there. A fine-grained matrix with large lapilli/small blocks, some of which have been brought up from greater than 70 metres depth, suggests that this deposit was emplaced in an explosive eruption with an origin deeper than 70 metres. No evidence for hydrothermal alteration was found in the sample. Cathodoluminescence of free quartz grains within the matrix suggests that the quartz has a volcanic origin, while microprobe analysis of glass attached to the quartz grains suggests that the Earthquake Flat Pyroclastics could be the origin.

Lack of hydrothermally altered material within the deposit suggests that there was no well-developed hydrothermal system present, and hence that the eruption was not of hydrothermal origin; it is therefore inferred to have been a phreatic eruption (after Mastin, 1991).

4.1.2 Okaro-B

The Okaro-B type locality is the road cut at the southwest edge of Lake Okaro (Grid Reference 1896625mE, 5755425mN). Okaro-B samples, from the measured section (Appendix H), are OU75047-OU75061.

4.1.2.1 Physical Description

Okaro-B is the most extensive deposit, being 0.1 metres thick at 700 metres west from the lake edge and approximately 6.5 metres thick at the lake edge. The eastern lakeshore is composed entirely of Okaro-B, with large blocks of welded ignimbrite present just below the 1886 paleosol.

The breccia is clast supported, with angular clasts in an ash matrix, and shows no internal lamination. Clast sizes range from lapilli through to blocks, with blocks up to 0.2 metres very common; a general horizon of very large, greater than 0.4 metres along a single axis, blocks occurs roughly 3 metres from the base of Okaro-B (see measured section in Appendix H), and blocks of this size can be found ejected out to approximately 400 metres from the lake edge (Figure 16). Clast composition differs from that in Okaro-A, with approximately 50% more clasts of welded ignimbrite than pumice; all of the very large blocks are welded ignimbrite. Clasts are generally unaltered, although faint blue- and red-stained clasts increase in abundance upwards in the section from just below the horizon where large blocks are common. The matrix is the same as that in Okaro-A.

Figure 16
Rangitaiki Ignimbrite ejecta block from Okaro-B phase – block measures 0.45x0.40 m, with impact-sag penetrating over 0.50 metres. Note distorted Kaharoa Ash to right of block.



4.1.2.2 Petrographic Description

Thin sections were made from the 2λ - 3λ fractions of samples OU75047, OU75050, OU75055, and OU75056, and from the 1λ - 2λ fractions of samples OU75047, OU75050, OU75055, OU75058, and OU75061.

Hematite staining is common on lithic fragments in all samples, although lithic fragments are too fine grained to identify, with rare leucoxene on some grains. Hydrothermal quartz, which differs from standard quartz since it forms as a precipitate from hydrothermal fluids as opposed to crystallizing from magmatic fluids or metamorphic

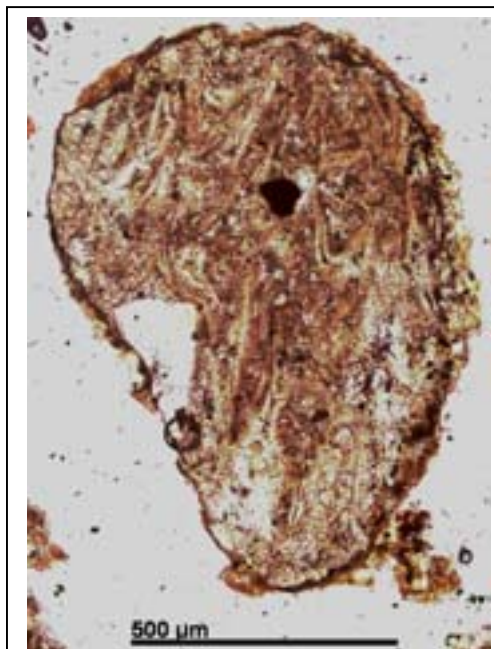


Figure 17
Hydrothermal quartz from OU75058 in plane polarised light (upper Okaro B)

recrystallization, is present in all thin sections (Figure 17), as are volcanic quartz, plagioclase, hornblende, biotite, orthopyroxene, clinopyroxene, glass and lithic fragments. An increase in the amount of hydrothermal quartz was observed going from OU75047 (less than 2% by visual estimate) to OU75061 (maximum of 10% by visual estimate).

4.1.2.3 Grainsize Analysis

Raw grain size data can be found in Appendix E. The Okaro-B samples (Table 4) exhibit wide variation (representative histograms in Figure 18, next page), but some patterns do become apparent. Overall, the deposit has an average graphic mean (after Folk, 1980) of -0.91λ , although this varies between -0.37λ (OU47049) and -1.95λ (OU47060), and is very poorly sorted with an inclusive graphic standard deviation of 2.09λ (1.84λ (OU75053) to 2.42λ (OU75054)). The deposit varies between near symmetrical (-0.01 for OU75052) and fine-skewed ($+0.29$ for OU75057), although there is no apparent progression from sample to sample. The deposit is mesokurtic, although some samples are leptokurtic (OU75052 and OU75056) or platykurtic (OU75058, 75059, 75060, and 75061).

A pattern becomes apparent when looking over the kurtosis values, with a shift from leptokurtic to mesokurtic from OU75052 (1.15) to OU75055 (0.92), and a shift from leptokurtic to platykurtic from OU75056 (1.21) to OU75060 (0.81). No additional pattern

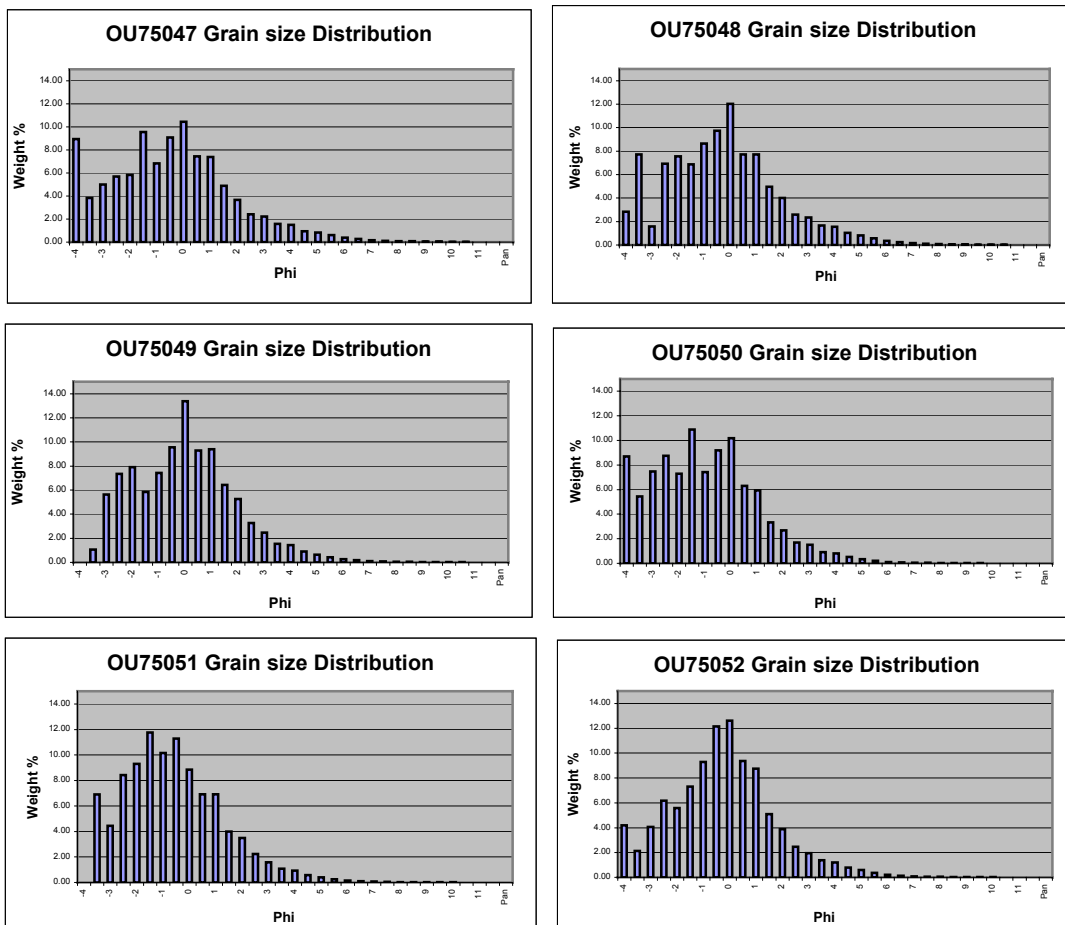
Lake Okaro: Explosions and Erosion

exists for OU75052 to OU75055; however, for OU75056 to OU75060, the inclusive graphic mean changes from -0.86λ to -1.82λ , representing an increase in grain size.

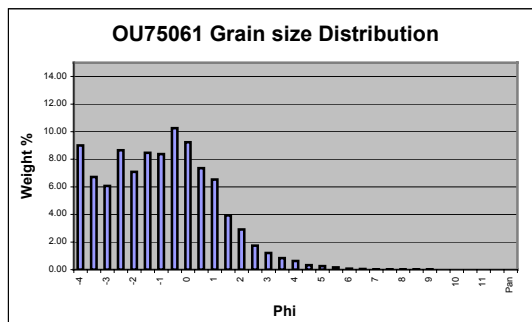
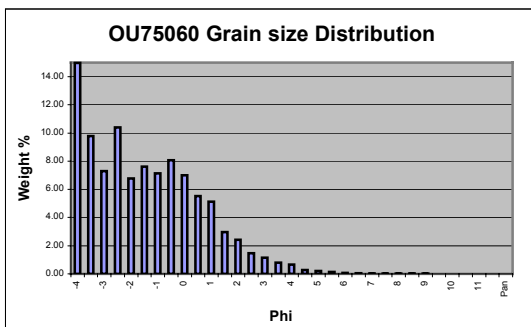
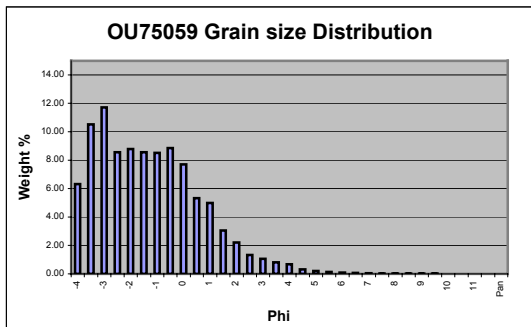
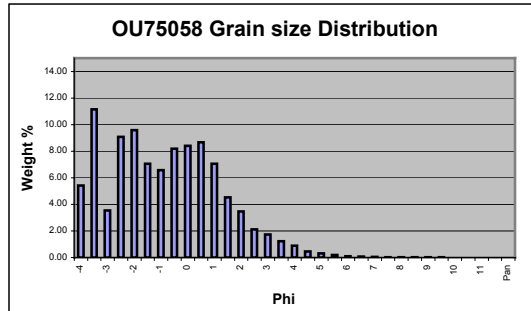
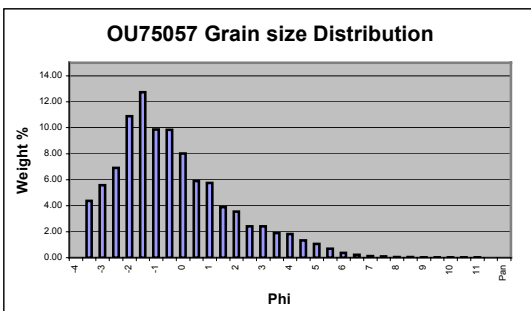
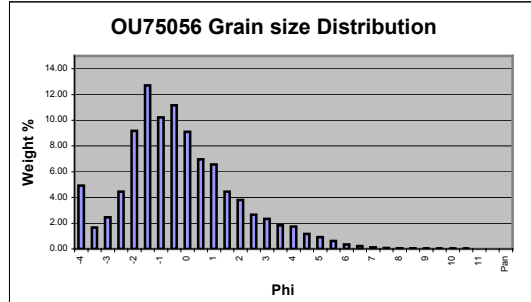
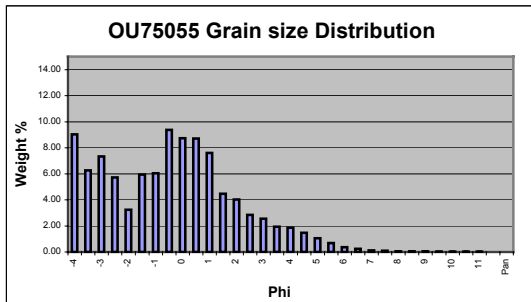
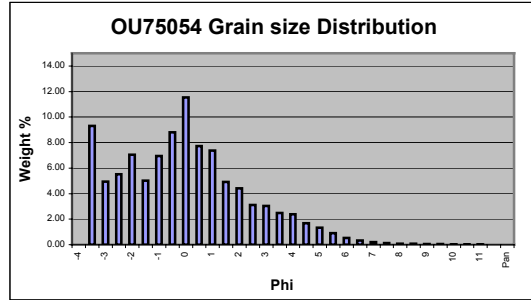
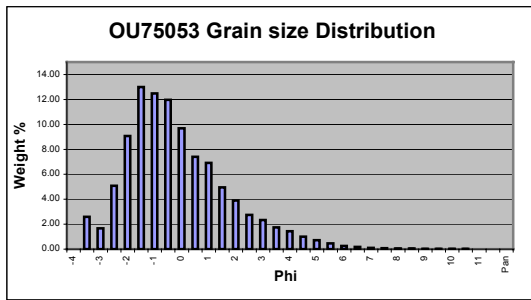
Table 4
Okaro-B grain size analysis graphical statistics (after Folk, 1980)

	OU75047	OU75048	OU75049	OU75050	OU75051
Graphic Mean	-0.85λ	-0.60λ	-0.37λ	-1.36λ	-0.95λ
Inclusive Graphic Standard Deviation	2.32λ	2.16λ	1.95λ	2.02λ	1.86λ
Inclusive Graphic Skewness	0.03	0.05	0.03	0.09	0.13
Graphic Kurtosis	1.05	1.07	0.99	0.97	1.02
	OU75052	OU75053	OU75054	OU75055	OU75056
Graphic Mean	-0.62λ	-0.49λ	-0.39λ	-0.81λ	-0.55λ
Inclusive Graphic Standard Deviation	1.98λ	1.84λ	2.42λ	2.50λ	2.12λ
Inclusive Graphic Skewness	-0.01	0.26	0.08	0.01	0.18
Graphic Kurtosis	1.15	1.07	1.00	0.92	1.21
	OU75057	OU75058	OU75059	OU75060	OU75061
Graphic Mean	-0.68λ	-1.25λ	-1.63λ	-1.82λ	-1.34λ
Inclusive Graphic Standard Deviation	2.12λ	2.12λ	1.91λ	2.06λ	2.01λ
Inclusive Graphic Skewness	0.29	-0.01	0.16	0.17	0.00
Graphic Kurtosis	1.09	0.88	0.87	0.81	0.90

Figure 18
Representative grainsize histograms for Okaro-B samples



Lake Okaro: Explosions and Erosion



4.1.2.4 Clay Analysis Using X-Ray Diffraction

XRD analysis (Appendix F) shows the presence of clay minerals in all samples from OU75047 to OU75060, with sericite in the lower samples and kaolinite and montmorillonite present in higher samples. Sample OU75061 contains jarosite and an aluminosilicate, but the species of aluminosilicate is indeterminate.

4.1.2.5 Interpretation

The presence of clay minerals suggests that either there may have been hydrothermal alteration occurring prior to eruption (sericite is a common low-grade hydrothermal mineral), or, more likely, that the area has been subjected to a high degree of weathering (as suggested by the presence of kaolinite and montmorillonite). The lack of hydrothermally altered clasts in the lower part of the deposit suggests that there was no input from a hydrothermal system, although the presence of hydrothermal quartz in all thin sections suggests that hydrothermal fluid could have been present. This is the dominant deposit at the south end of the lake, and is thus inferred to have originated there, quite likely from the same crater as Okaro-A.

If the Okaro-A crater was also the origin for Okaro-B, then either the absence of hydrothermal material in Okaro-A or the presence of hydrothermal material in Okaro-B must be explained (see Section 4.3.1 below).

4.1.3 Okaro-C

The Okaro-C type locality is an outcrop on the Landcorp Rotomahana farm to the north of Lake Okaro (Grid Reference 1896950mE, 5756050mN). Okaro-C samples, from the measured section (Appendix H), are OU75062- OU75066. Deposits represented by sample OU75066 are only found at the road cut at the southwest edge of Lake Okaro (Grid Reference 1896625mE, 5755425mN).

4.1.3.1 Physical Description

Okaro-C can be hard to distinguish from Okaro-B in the road-cut where the section was measured (see Appendix H); there appears to be a gradual transition. Okaro-C can easily be distinguished from Okaro-B at the north and south ends of the lake, where Okaro-C appears to have an almost rhythmic layering (~0.3 metre scale) in addition to a reddish stain to the matrix (Figure 19, next page). The proportion of welded-ignimbrite clasts decreases relative to pumice, and there is an increase in blue- and red-stained clasts. Maximum clast size is approximately 0.1 metres, but unlike Okaro-A, which is definitely



matrix supported, Okaro-C is framework supported by predominantly lapilli sized fragments.

The matrix is similar in composition to that Okaro-A, but feels more clay-rich and cohesive. The upper 0.5-0.75 metres of Okaro-C becomes exceptionally fine-grained with no larger clasts present, appearing like a loose sand until it is rubbed when it shows itself to be weakly aggregated fine ash. The composition of the ash (under binocular microscope) appears the same as the rest of the matrix.

Okaro-C has a variable thickness, with at least 2 metres of breccia on top of the hills at the north and south ends of the lakes (the ash is not present in these locations), and approximately 2.5 metres in the road-cut for the measured section (where the ash was observed). The overall thickness is thus interpreted to be roughly 3 metres (on the assumption that the ash was eroded off the hill-tops). The lateral extent of Okaro-C is harder to interpret, with 0.1 metres of fine breccia 500 metres north of the lake and some mixing between it and Okaro-B to the west. Breccia outcrop around the eastern shore of the lake shows no sign of Okaro-C.

4.1.3.2 Petrographic Description

Thin sections were made from the 2 λ -3 λ fractions of sample OU75064, and from the 2 λ -3 λ fractions of OU75065. No thin sections were attempted from OU75066 because the material was too fine-grained to make satisfactory grain mounts.

There is a large amount of hematite present as a stain to most grains, along with leucoxene, and there is an increase in the number of lithic and hydrothermal quartz fragments. Quartz and plagioclase dominate the assemblage, but biotite, hornblende, clinopyroxene, orthopyroxene, glass and lithic fragments (welded ignimbrite?) are also present. Grains in OU75065 show extreme alteration of quartz and feldspar, with quartz grains exhibiting an uneven, corroded texture and feldspars showing alteration laminae at approximately 30° to the twinning.

4.1.3.3 Grainsize Analysis

Full grain size data can be found in Appendix E. The Okaro-C samples (Table 5, representative histograms in Figure 20 on next page), with the exception of OU75066, represent, after Folk (1980), a poorly sorted (1.74 λ to 1.89 λ inclusive graphic standard deviation), coarse-grained (graphic mean between -0.94 λ and -1.13 λ), near symmetrical to fine-skewed (+0.02 to +0.16), mesokurtic deposit (graphic kurtosis between 1.02 and 1.10). OU75066 is very different from the rest of the deposit; while remaining poorly sorted, it is fine-grained, fine-skewed, with a leptokurtic graphical kurtosis.

4.1.3.4 Clay Analysis Using X-Ray Diffraction

XRD analysis (Appendix F) showed the presence of either kaolinite or montmorillonite in every sample. Sample OU75062 contains jarosite and montmorillonite.

4.1.3.5 Interpretation

Distribution of Okaro-C predominantly to the north of the lake suggests a source in that area. The apparent layering suggests either multiple events or multiple sources. The presence of obviously hydrothermally altered material suggests that this was erupted from a hydrothermal system. The presence of clay minerals is not indicative of either hydrothermal origin or weathering, although the nature of alteration of minerals (eg, the

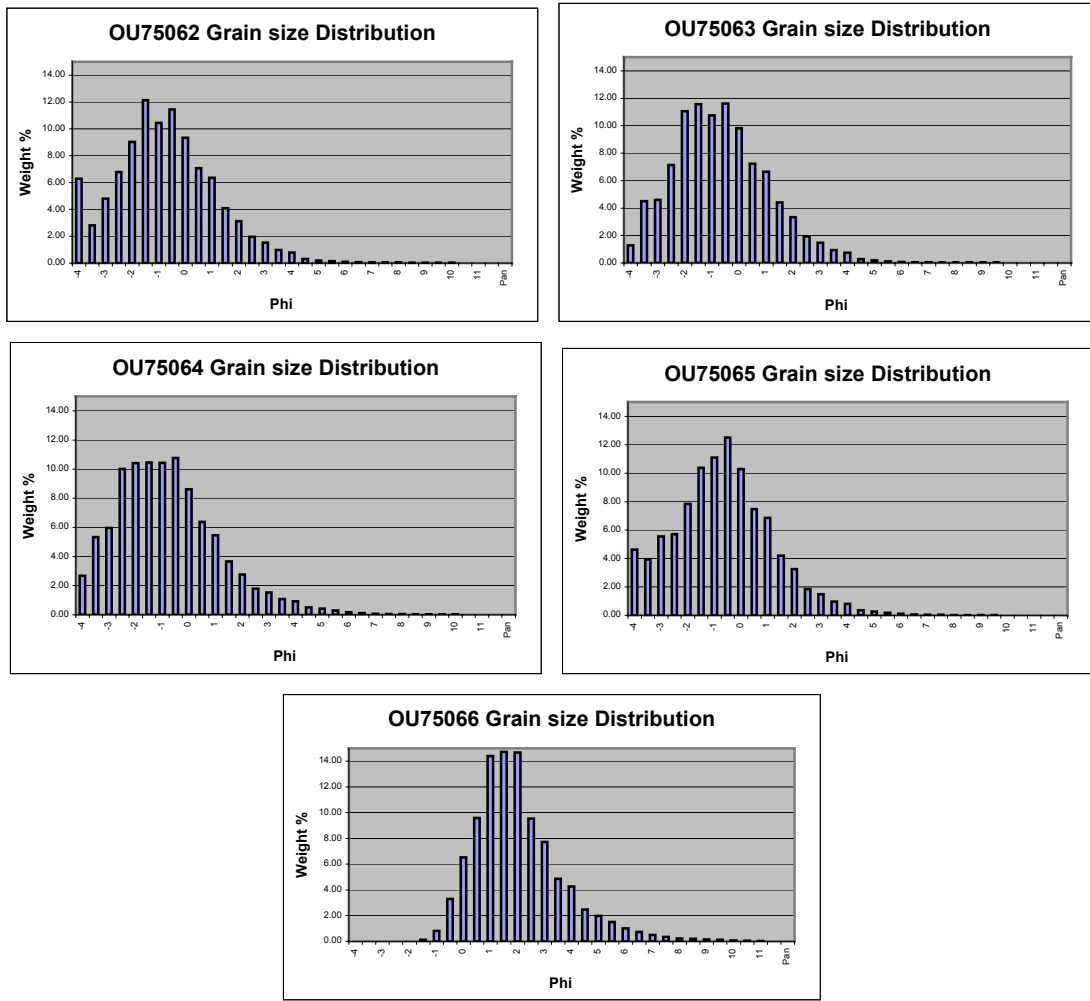
Table 5

Okaro-C grain size graphical statistics (after Folk, 1980)

	OU75062	OU75063	OU75064	OU75065	OU75066
Graphic Mean	-1.05 λ #	-0.94 λ	-1.13 λ	-0.99 λ	1.68 λ
Inclusive Graphic Standard Deviation	1.89 λ	1.74 λ	1.88 λ	1.87 λ	1.57 λ
Inclusive Graphic Skewness	0.06	0.11	0.16	0.02	0.22
Graphic Kurtosis	1.10	1.02	1.06	1.09	1.16

Lake Okaro: Explosions and Erosion

Figure 20
Representative histograms for Okaro-C samples



texture of feldspars in Figure 21, next page) in thin section does suggest a hydrothermal origin. This deposit, then, is assumed to be from hydrothermal eruptions centred in the

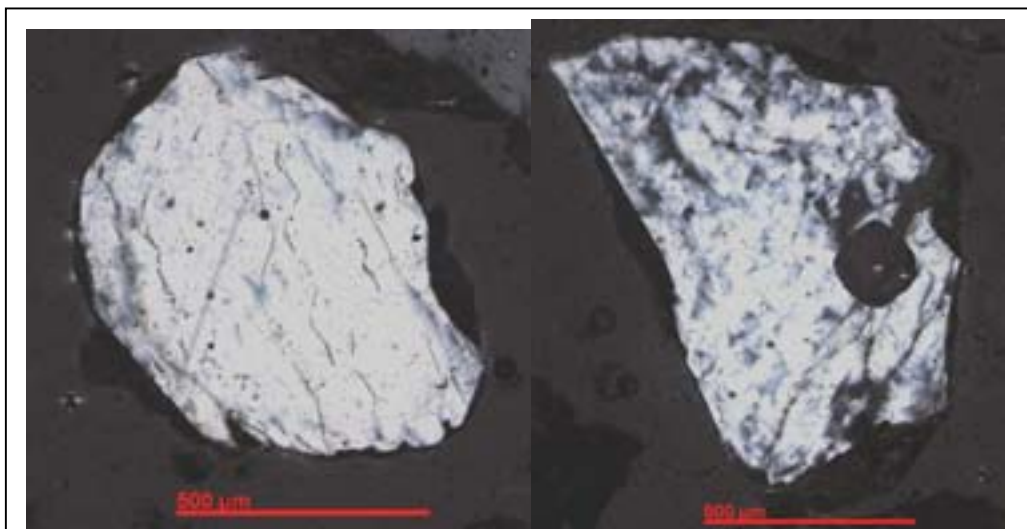


Figure 21
Cross-polarised light images of two feldspar grains from OU75065. Note the 'dirty' texture associated with alteration mineralization.

area now occupied by the northern section of Lake Okaro.

4.2 Distribution and Volume

The Okaro-C breccia can be found 0.10 metres thick as part of the current paleosol at a distance of approximately 950 metres west from the centre of Lake Okaro, has a maximum thickness at the south-southwest end of the lake of approximately 11.5 metres, and is at least 4 metres thick at the north end of the lake. The land to the east and south of Lake Okaro is dominated by pasture, and very little outcrop can be found except around the shore of the lake. The Rotomahana Mud thickens to the north of Lake Okaro, reducing outcrop of underlying Okaro beds. These observations are very similar to those made by Cross (1963) except that the extent of the deposit observed has been reduced (1300 metres as opposed to roughly 1000 metres), most likely due to extensive farming in that area in the intervening time. Because of this loss of information, the volume estimate made by Cross (1963) better represents the original dimensions of the deposit, and will be used here.

4.3 Interpretation

The volume of Lake Okaro is large, at approximately $4.4 \times 10^6 \text{ m}^3$, but that volume is spread over an area 500 metres by 700 metres to an average depth of 12.5 metres. The amount of ejecta from the craters is $3.67 \times 10^6 \text{ m}^3$, which easily fits into this volume, but the depth of excavation must extend to greater than 70 metres, and slumping alone cannot explain the shape of the lake.

4.3.1 Eruption episodes

The presence of three distinct units within the Okaro-Breccia, and their geometrical arrangement, suggests that there have been three phases to the development of Lake Okaro (see Appendix I for schematic interpretation of events):

Phase 1: Eruption of Okaro-A from an initial ‘throat-clearing’ event focused at a depth greater than 60 metres and rupturing through the Rangitaiki Ignimbrite at the south end of the present lake (Appendix I, Steps 2 & 3). This deposit is dominated by fine-grained material with rare clasts from the Rangitaiki Ignimbrite being present (thus fixing the minimum depth). The size of the ignimbrite clasts (<60mm) suggests that, while being explosive, large volumes of material remained within the crater (either from the erupted material slumping back in or from the eruption not having the energy to completely expel

large clasts). Lack of hydrothermal alteration in clasts and matrix (in thin section and XRD) suggests that this phase did not originate within a hydrothermal system.

Phase 2: Eruption of Okaro-B from the same crater as Okaro-A (Appendix I, Steps 4 & 5). Material that was not ejected from the crater during the Okaro-A eruption was remobilised during the Okaro-B event, with additional fragmentation of the wall-rock from escaping steam widening the vent. Since the 50+ metres of Earthquake Flat Pyroclastics overburden had been removed, large blocks of Rangitaiki Ignimbrite could now be thrown clear of the crater. The presence of hydrothermal quartz in thin section suggests that this phase did involve disruption of hydrothermally altered ground, indicating a "hydrothermal" eruption, and this may be explained by the intersection of the Okaro-A crater with a hydrothermal system (where the Okaro-C phase originated), or by an overlap between the Okaro-B and Okaro-C phases (this is the preferred explanation). A change in eruption intensity between the Okaro-A and Okaro-B phases would have had to occur to explain the visual differences between them, and could explain the observed parallel laminations of iron staining at the top of Okaro-A.

Phase 3: This was not a single event, but rather represents a number of smaller, localised eruptions. Multiple deep points on the lake floor suggest a number of small craters developed in the area now occupied by the northern part of the lake. The limited distribution and layered deposits of Okaro-C material, being present more to the north than the south of the lake, suggests that the majority of secondary events occurred after the paroxysmal Okaro-B event. The presence of hydrothermally altered material in all samples suggests that this phase was from hydrothermal eruptions, and potentially represents reworking of Okaro-B material. If there had been a shallow hydrothermal system to the north of the lake, then sudden burial during the deposition of Okaro-B could result in localised increases of pressure from burial (an additional 3-4 metres of saturated material with a density of $\sim 2.15 \times 10^3 \text{ kg/m}^3$ would add approximately 86 kPa of overburden pressure), this could then form hydrothermal eruptions with the observed distribution by restricting the escape of steam from an already overstressed hydrothermal system; these would be 'progressive flashing' eruptions, which would be shallowly seated and would terminate once the pressure was equalised. This would also account for the presence of unaltered Rangitaiki Ignimbrite and Earthquake Flat Pyroclastics in combination with altered material in the Okaro-C deposits. Some other consequences of this is that it could also explain the presence of altered material in the upper portion of the Okaro-B deposit, as well as excavating the northern end of the present lake to its present

geomorphology and partially filling the Okaro-A/B crater (Appendix I, Step 6). If these small eruptions were to have occurred concurrent with Okaro-B, then this would also explain the presence of initially low, then increasing, amounts of hydrothermal quartz in Okaro-B.

4.3.2 Eruption mechanism

Of the eruption types listed by Browne & Lawless (2001), no single one could explain all observed features within the Okaro deposits. The presence of Rangitaiki Ignimbrite in the initial deposits suggests an explosive eruption from depth, perhaps with a simple “cap-rock rupture” mechanism. This, however, is only for the initial phase that resulted in the deposition of Okaro-A. Interestingly, the absence of hydrothermal alteration within Okaro-A suggests that this was not a hydrothermal eruption. Instead, the Okaro-A eruption was apparently a phreatic one, possibly triggered by basaltic intrusion as postulated by Nairn et al (2004).

Okaro-B most likely was a more standard ‘progressive flashing’ eruption within the material disrupted during the Okaro-A phase. There is a dramatic increase in the amount of coarse clasts at this stage, suggesting that less energy was going into fragmentation and more into mobilisation of the material, helping support the idea that Okaro-A shattered a path to the surface. This phase would likely have consisted of a fairly continuous stream of material being emitted, with occasional larger eruptions as evidenced by the presence of a layer of large blocks in the middle of the deposit. Large blocks of Rangitaiki Ignimbrite (assumed density $2 \times 10^3 \text{ kg/m}^3$) from at least 60 metres depth have been thrown approximately 700 metres from the centre of the hypothesised vent location; an initial velocity of $\sim 110 \text{ m/s}$ on a 45° ejection angle would be needed for this, while if the angle was increased to 60° the required initial velocity would be $\sim 120 \text{ m/s}$ (velocities determined using the ballistics calculator ‘Eject’ from the United States Geological Survey).

The Okaro-C phase eruptions are all likely to be from the restriction of steam release from an already overstressed hydrothermal system resulting in a number of ‘progressive flashing’ hydrothermal eruptions. Draining of water from a hydrothermal reservoir during the Okaro-A and B events, lowering the boiling point within the reservoir and thus increasing the steam pressure beneath the freshly deposited Okaro-B layer. These would have occurred immediately after, and possibly during, the Okaro-B eruption(s), and could explain the presence of hydrothermally altered clasts within the Okaro-B deposit.

4.3.3 Summary

Lake Okaro was formed by an initial phreatic eruption at the south end of the lake, followed by a series of much smaller hydrothermal eruptions in the north end of the lake, which dammed a stream flowing through the area (see Appendix I for a schematic interpretation of the eruption progression, and Appendix K for presumed pre-eruption geography) The presence of hydrothermal fluids at 40 metres depth in the Environment Bay of Plenty well drill-hole (Shane Burchell, pers. comms. 2005), being above the Rangitaiki Ignimbrite and within the Earthquake Flat Pyroclastics, would allow for the development of a pressurised steam-zone beneath the extensive Okaro-B deposit allowing for small hydrothermal eruptions to form.

The presence of undercutting to the north and terracing to the east of Lake Okaro suggests that lake level was once much higher (approximately 3 metres), until such a time as the lake eroded through the hydrothermal deposit to the level of the present drainage (which appears to have not migrated much). A 50-metre breach in the terrace at the southeast end of the lake suggests that this may have been a catastrophic failure (stereoscopic projection of oblique aerial photographs also suggests that this may have occurred); further work could be done in order to determine if this were the case, although after 50+ years of farming the evidence would be very difficult to find.

5 Discussion

The identification of Lake Okaro as a hydrothermal eruption crater (Cross, 1963; Hedenquist & Henley, 1985; Nairn et al, 2004) is slightly misleading because, while there is some hydrothermal material in the deposit, the presence of material from the deepest source and absence of hydrothermal material in the initial phases suggest a phreatic origin. Hydrothermal eruptions have occurred in the Okaro area, but these were centred to the north end of the present lake, and consisted of a number of small events occurring concurrently and after the final phase of the phreatic eruption. The initial phreatic eruption was small, but fragmented a large (~220 metre) area to ~90 metres depth (Appendix J); much of the large material was not ejected at this time. The eruption disrupted a hydrothermal field, which resulted in the migration of fluids into the fragmented area prompting a second, hydrothermal-steam-generated, phase of eruption. This excavated much of the fragmented material from the first eruption and creating a crater. Disruption to the hydrothermal system, coupled with burial by the second phase eruption, prompted a number of shallow hydrothermal eruptions to the north of Lake Okaro, which redistributed material and partially filled in the phreatic/hydrothermal eruption crater. The area affected by cratering and slumping during these events was slightly smaller than that of the present lake, although the main stream (entering the present lake from the west) was blocked by ejecta from the eruptions, causing a natural dam to form and undercutting the hills to form cliffs at the north end of the lake. Prior to this event, Lake Okaro did not exist.

There is a problem with the idea of an initial blast initiating at a depth of ~70 metres, and that is the amount of energy needed to remove that much overburden. The presence of Rangitaiki Ignimbrite in the initial stages (the first clasts are found approximately 0.25 metres into the deposit) suggests that the eruption initiated quite deep, but the fine grain size suggests that it must have had a localised effect and that much of the energy went into fragmentation instead of excavation. Using an overburden density of $2.15 \times 10^3 \text{ kg/m}^3$ and a depth of 70 metres, the initial eruption has to have had enough energy to fragment, at a minimum, $1.5 \times 10^5 \text{ kg/m}^2$ of overburden (assuming vertical sides to the explosion column). Thus the explosion would have to overcome a pressure of 1.48 MPa in order to reach the surface. However, this pressure is small compared to the pressure required to rupture the Ignimbrite in the first place. Assuming a minimum uniaxial compressive

strength of 15 MPa (Quane & Russell, 2003) for the Rangitaiki Ignimbrite, the explosion would have had to generate more than 16.48 MPa initially.

Nairn et al. (2004) favour the hypothesis that an arrested basaltic dyke intruded beneath the Ngapouri Fault, thus providing a CO₂ and heat pulse to trigger the eruptions. As a trigger, CO₂ alone would be unable to create the observed features. Basaltic intrusion beneath Mount Tarawera initiated the Kaharoa eruption (Leonard et al, 2002), the majority of basalt erupted had either a rhyolite coating or was an inclusion within rhyolite. With an intrusion length of 23 km, a dyke trending 052° (which is very close to the strike of the Ngapouri Fault) could intrude below the area from Waiotapu to Tarawera. This intrusion would breach the surface where possible (i.e., it could fracture propagate through any brittle igneous material underlying Tarawera) but over the majority of the area, where the rocks are either poorly consolidated or loose, the dyke would be arrested at depth.

Assuming that an arrested basalt dyke 23 km in length was the driving force behind the initial Okaro eruption (as postulated by Nairn et al. 2004), an estimate for the amount of heat (and hence energy) released into the system can be made. If the basalt dyke was a similar thickness to that driving the AD1886 Tarawera eruption, 2 metres (Nairn & Cole, 1981), the dyke was arrested at a depth greater than 500 metres (since no juvenile clasts have been found in any of the Waiotapu eruptions, with the deepest bringing material up from ~350 metres; Hedenquist & Henley, 1985), and the dyke was losing heat from the base of the seismogenic zone at ~7 km where it entered the convective heat-loss regime (Rowland & Sibson, 2004), then this gives a total volume (v) of $2.76 \times 10^8 \text{ m}^3$ of basalt available for cooling. With an initial typical basalt temperature (T) of $\sim 1200^\circ\text{C}$ and a thickness of 2 metres, the dyke would cool to 325°C (when water would no longer boil at 500 metres depth, causing steam generation to follow normal boiling temperature gradients) over a matter of hours to days (Carrigan, 2000). This would release 9.17×10^{17} Joules of energy (assuming a specific heat capacity (c) of 1.45 kJ/kg.K and a density (ψ) of 2600 kg/m^3 for basalt; Spera, 2000) based on the enthalpy (H) of the dike (where $H = (c\Delta T + L)\Delta(v\Delta\psi)$ and the latent heat (L) = 0 due to the dyke being arrested at depth and thus no heat being lost on eruption).

With $3.67 \times 10^6 \text{ m}^3$ of material ejected at an approximate density of $2.15 \times 10^3 \text{ kg/m}^3$, roughly $7.89 \times 10^9 \text{ kg}$ of material was ejected from the area now occupied by Lake Okaro (this is higher than the mass estimated by Cross (1963), and is estimated based on crystal

content of the matrix; Cross did not provide a density estimate for the Okaro Breccia, only a total mass estimate of 4.2×10^6 tons). The amount of energy ($E_{k:debris}$), using the formula: $E_{k:debris} = \frac{1}{2}mv^2$, with a velocity (v) from the large blocks of 115 m/s, required to mobilise this mass (m) is 5.22×10^{13} Joules; halving the velocity to provide an average value for the matrix still requires 1.3×10^{13} Joules to mobilise the ejecta. Mastin (1991) notes that the amount of energy used in fragmentation during an eruption is typically between 1×10^{-3} and 1×10^{-2} of the total energy released during an eruption; this would suggest that the total energy released by the Okaro eruptions would be $\sim 1.3 \times 10^{15}$ Joules; the energy released in the Okaro eruptions would thus represent less than 0.1% of the total energy released from an arrested basaltic dyke (9.17×10^{17} Joules). This value of energy release is also consistent with experimentally determined values for the amount of energy required to form craters of approximately 200 metres diameter (Goto et al. 2001).

Experimentally determined amounts for energy release from magma-water interactions (Zimanowski et al. 1995) suggest that the pressures generated during phreatomagmatic eruptions could be as high as 100 MPa. The Okaro eruptions are not phreatomagmatic, however, and thus the pressure generated from interaction of a dyke with groundwater would be less due to being limited to the rate of convective heat transfer. That being said, however, even if the pressure was only 1/5 that value, 20 MPa is still greater than the 16.48 MPa necessary to rupture the Rangitaiki Ignimbrite below 60 metres of Earthquake Flat Pyroclastics and covering tephra.

After the eruptions, a small river running through the area dammed by ejecta formed the present Lake Okaro in the partially filled craters. Lake Okaro reached a maximum depth of approximately 3 metres greater than its present level before breaching the ejecta dam through a 50-metre rupture in a breakout flood, lowering to its present level; the timing of this event is unknown, but would likely have occurred within 100 years of the event (best estimate). Further work could be made into this, but due to intensive farming in the area most near-source indicators of a breakout flood will be impossible to detect.

6 Conclusions

- 1) Rill erosion took place entirely within the Rotomahana Mud, started within days of the AD1886 eruption, and terminated within a short number of years after the eruption. This appears to be a common erosional response to volcanic eruptions, or any other action, such as wildfire, that removes/covers vegetation from hills, worldwide.
- 2) Rill complexity is greatest at the heads of valleys, with overall catchment complexity increasing where valleys meet.
- 3) Why rill erosion ceased is unknown but is likely related to the permeability of the strata, whereby rill erosion slows down as the strata becomes more permeable (this would be due to absorption of water by the strata as opposed to mobilising the surface of it). No experimental studies have been found that specifically investigate this, but a laboratory experiment involving sprinkler systems and materials of varying permeability could be devised to test this hypothesis.
- 4) Lake Okaro was formed by number of eruptions, with the initial eruption being phreatic and located at the south end of the present lake.
- 5) The phreatic eruption initiated at a depth of at least 60 metres, and would have excavated an eruption vent approximately 200 metres across.
- 6) Following the initial stage of the phreatic eruption, at least 3 small hydrothermal eruptions occurred in the area occupied by the north end of the present lake. These hydrothermal eruptions continued after cessation of the phreatic eruption, partially filling the phreatic eruption vent with remobilised material, and depositing a mixture of altered and unaltered material.
- 7) The amount of energy needed to form the Okaro eruptions is approximately 1.3×10^{15} Joules, which could have been supplied from the heating of groundwater by intrusion of a basaltic dyke along the Ngapouri Fault during the second stage of the Kaharoa eruptive episode at Tarawera.
- 8) Ejecta from the eruptions dammed a small river, which filled the craters and formed a lake larger than the present Lake Okaro. Failure of the ejecta dam in a 50-metre rupture lowered the lake down to its present level.

7 References

- €# Bixley, P.F., & Browne, P.R.L. (1988). *Hydrothermal Eruption Potential in Geothermal Development*. In: Proceedings of the 10th New Zealand Geothermal Workshop, Auckland University Geothermal Institute, 1988, p.195-198
- €# Browne, P.R.L., & Lawless, J.V. (2001). *Characteristics of hydrothermal eruptions, with examples from New Zealand and elsewhere*. Earth-Science Reviews 52: 299-331
- €# Carrigan, C.R. (2000). *Plumbing Systems*. In: Encyclopedia of Volcanoes (Ed. by H. Sigurdsson, B. Houghton, S. McNutt, H. Rymer, & J. Stix), Academic Press, New York
- €# Collar, R.J., & Browne, P.R.L. (1985). *Hydrothermal Eruptions at the Rotokawa Geothermal Field, Taupo Volcanic Zone, New Zealand*. In: Proceedings of the 7th New Zealand Geothermal Workshop, Auckland University Geothermal Institute, 1985, p.171-175
- €# Collins, B.D., Dunne, T. (1986). *Erosion of Tephra from the 1980 eruption of Mount St. Helens*. Geological Society of America Bulletin 97: 896-905
- €# Cross, D. (1963). *Soils and Geology of some Hydrothermal Eruptions in the Waiotapu District*. New Zealand Journal of Geology and Geophysics 6:70-87
- €# Folk, R.L. (1980) *Petrology of Sedimentary Rocks*. Hemphill Publishing Company, Austin, Texas.
- €# Glicken, H. (1996). *Rockslide-Debris Avalanche of May 18, 1980, Mount St. Helens Volcano, Washington*. Open File Report 96-677, United States Geological Survey. 98 p.
- €# Goto, A., Taniguchi, H., Yoshida, M., Ohba, T., & Oshima, H. (2001). *Effects of Explosion Energy and Depth to the Formation of Blast Wave and Crater: Field Explosion Experiment for the Understanding of Volcanic Explosion*. Geophysical Research Letters 28(22): 4287-4290
- €# Götze, J., Plötze, M., & Habermann, D. (2001). *Origin, spectral characteristics and practical applications of the cathodoluminescence (CL) of quartz – a review*. Mineralogy and Petrology 71: 225-250
- €# Grange, L.I. (1937). *The Geology of the Rotorua-Taupo Subdivisions*. New Zealand Geological Survey Bulletin 37. 138 p.
- €# Hedenquist, J.W., & Henley, R.W. (1985). *Hydrothermal Eruptions in the Waiotapu Geothermal System, New Zealand: Their Origin, Associated Breccias, and Relation to Precious Metal Mineralisation*. Economic Geology 80: 1640-1668
- €# Irwin, J. (1974). *Lake Okaro and Lake Ngapouri provisional bathymetry: New Zealand Oceanographic Institute Chart, Lake Series 1:3168*. New Zealand Oceanographic Institute
- €# Keam, R.F. (1988). *Tarawera: The Volcanic Eruption of 10 June 1886*. R.F. Keam, Physics Department, University of Auckland. 472 p. ISBN 0-473-00444-5
- €# Leonard, G.S., Cole, J.W., Nairn, I. A., & Self, S. (2002). *Basalt triggering of the c. AD 1305 Kaharoa rhyolite eruption, Tarawera Volcanic Complex, New Zealand*. Journal of Volcanology and Geothermal Research, 115: 461-486
- €# Lloyd, E.F. (1959). *The Hot Springs and Hydrothermal Eruptions of Waiotapu*. New Zealand Journal of Geology and Geophysics 2: 141-176

Lake Okaro: Explosions and Erosion

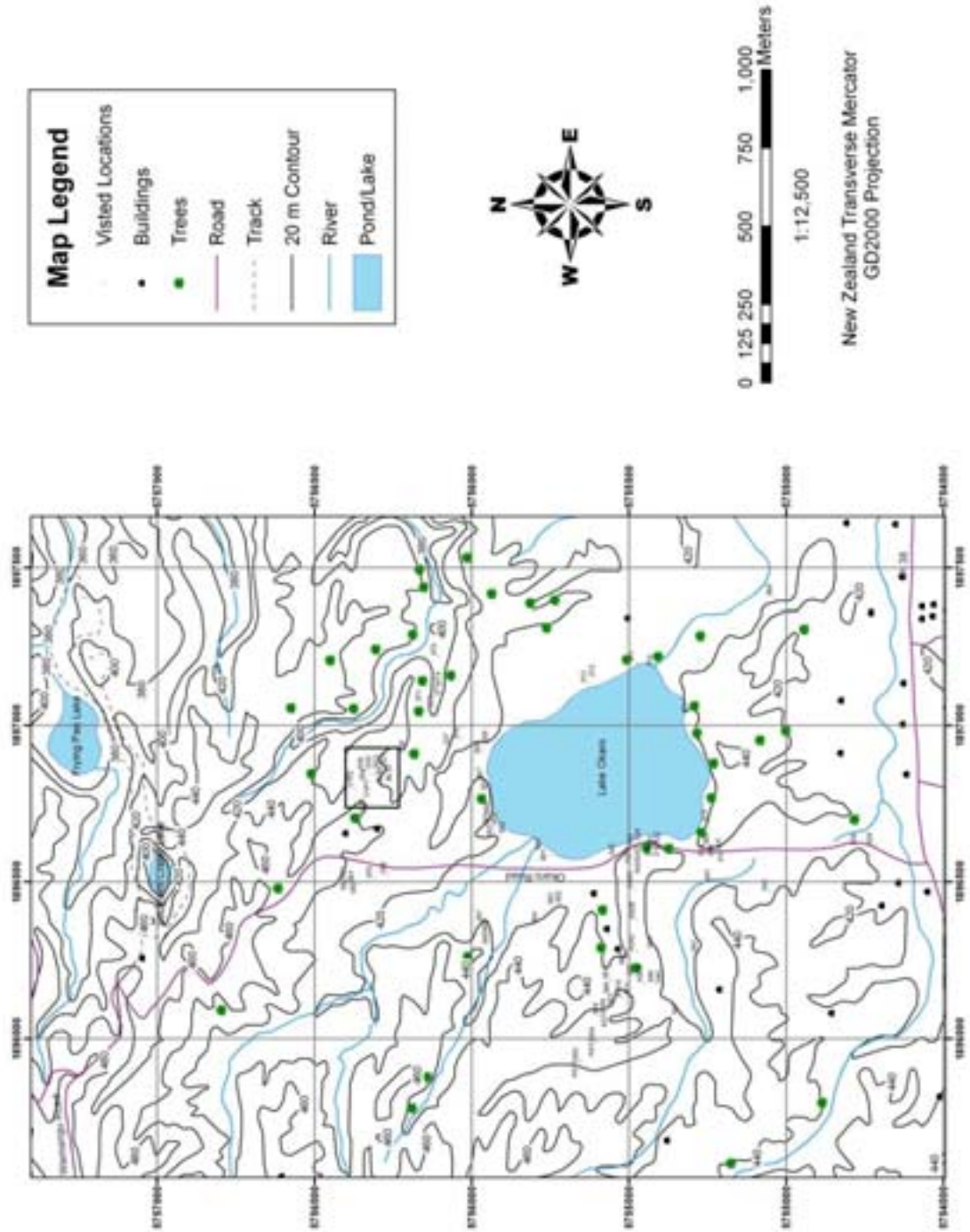
- €# McIntosh, J. (2003). *Lake Okaro-Catchment Management Draft Working Paper*. Environment Bay of Plenty Environmental Publication 2003/17. 23 p. Environment Bay of Plenty, Whakatane, New Zealand.
- €# Manville, V., & Wilson, C.J.N. (2004). *The 26.5 ka Oruanui eruption, New Zealand: a review of the roles of volcanism and climate in the post-eruptive sedimentary response*. *New Zealand Journal of Geology and Geophysics* 47: 525-547
- €# Mastin, L.G. (1991). *The roles of magma and groundwater in the phreatic eruptions at Inyo Craters, Long Valley Caldera, California*. *Bulletin of Volcanology*, 53: 579-596
- €# Nairn, I.A. (2002) *Geology of the Okataina Volcanic Centre, scale 1:50000*. Institute of Geological and Nuclear Sciences Geological Map 25. 1 sheet + 156 p. Institute of Geological and Nuclear Sciences, Lower Hutt, New Zealand.
- €# Nairn, I.A. (2003). *Stratigraphy of water supply well drilled at Lake Okaro in November 2003*. Unpublished report for Environment Bay Of Plenty. 3 p.
- €# Nairn, I.A., & Cole, J.W. (1981). *New Zealand Journal of Geology and Geophysics* 24: 585-592
- €# Nairn, I.A., & Wiradiradja, S. (1980). *Late Quaternary Hydrothermal Explosion Breccias at Kawerau Geothermal Field, New Zealand*. *Bulletin of Volcanology* 43(1): 1-13
- €# Nairn, I.A., Hedenquist, J.W., Villamor, P., Berryman, K.R., & Shane, P.A. (2004). *The ~AD1315 Tarawera and Waiotapu eruptions, New Zealand: contemporaneous rhyolite and hydrothermal eruptions driven by an arrested basalt dike system?* *Bulletin of Volcanology* 67(2): 186-193
- €# Ollier, C.D., & Brown, M.J.F. (1971). *Erosion of a young volcano in New Guinea*. *Zeitschrift fur Geomorphologie* 15: 12-28
- €# Prossler, I.P., & Williams, L. (1998). *The effect of wildfire on runoff and erosion in native *Eucalyptus* forest*. *Hydrological Processes* 12: 251-265
- €# Quane, S.L., & Russell, J.K. (2003). *Rock Strength as a metric of welding intensity in pyroclastic deposits*. *European Journal of Mineralogy* 12: 855-864
- €# Rosseel, J-B. (2002). *Magma-water interactions in a geothermal environment, the 1886 Rotomahana eruption*. Abstracts & Programme, GSNZ Annual Conference "Northland 2002", Geological Society of New Zealand Miscellaneous Publication 112A, p.50
- €# Rowland, J.V., & Sibson, R.H. (2004). *Structural controls on hydrothermal flow in a segmented rift system, Taupo Volcanic Zone, New Zealand*. *Geofluids* 4: 259-283
- €# Strahler, A.N. (1957). *Quantitative Analysis of Watershed Geomorphology*. *Transactions, American Geophysical Union*, 38(6): 913-920
- €# Scott, K.M., Janda, R. J., de la Cruz, E. G., Gabinete, E., Eto, I., Isada, M., Sexon, M., & Hadley, K. (1996). *Channel and Sedimentation Responses to Large Volumes of 1991 Volcanic Deposits on the East Flank of Mount Pinatubo*. In: *Fire and Mud: Eruptions and Lahars of Mount Pinatubo, Philippines* (Newhall & Punongbayan Eds.), University of Washington Press, Seattle and London. 1126 p.
- €# Segerstrom, K. (1950). *Erosion Studies at Paricutin, State of Michoacan, Mexico*. *Geological Survey Bulletin* 965-A. United States Geological Survey

Lake Okaro: Explosions and Erosion

- €# Segschneider, B. (2000). *Resedimentation of the 1.8 ka Taupo ignimbrite in the Hawke's Bay region, North Island, New Zealand*. Unpublished PhD Thesis, University of Otago
- €# Simmons, S.F., Keywood, M., Scott, B.F., & Keam, R.F. (1993). *Irreversible change of the Rotomahana-Waimangu hydrothermal system (New Zealand) as a consequence of a volcanic eruption*. *Geology* 21: 643-646
- €# Spera, F.J. (2000). *Physical Properties of Magma*. In: *Encyclopedia of Volcanoes* (Ed. by H. Sigurdsson, B. Houghton, S. McNutt, H. Rymer, & J. Stix), Academic Press, New York
- €# Zimanowski, B., Frohlich, G., Lorenz, V. (1995). *Experiments on steam explosion by interaction of water with silicate melts*. *Nuclear Engineering and Design* 155: 355-343

8.2 Appendix B – Okaro-Area Base Map

Sample Location Map for Lake Okaro Area



Lake Okaro: Explosions and Erosion

8.3 Appendix C – Outcrop and Sample Data

Outcrop	NZMG		NZTM		OU Samples	Description
	Easting	Northing	Easting	Northing		
001	2806692	6317283	1896583	5755756		Lake Okaro carpark
002	2806762	6317437	1896653	5755910		Bank ~150 m NNE of Okaro carpark
003	2806780	6317453	1896671	5755926		Bank ~165 m NNE of Okaro carpark
004	2806790	6317451	1896681	5755924		Bank ~175 m NNE of Okaro carpark
005	2806807	6317465	1896698	5755938		North edge of gully mouth
006	2806825	6317463	1896716	5755936		Lake edge
007	2806923	6317471	1896814	5755944		Exposure in bank NW shore of lake S of small inlet stream
008	2807029	6317492	1896920	5755966		Exposure in bank NW shore of lake N of small inlet stream
009	2807051	6317468	1896942	5755942		Cliffs NW lake edge
010	2807292	6316943	1897184	5755416		Exposure in bank SE shore of lake S of outlet stream
011	2807310	6317004	1897202	5755477		~50 m N of outlet stream in bank near lake edge
012	2807261	6317137	1897153	5755611		Small double box gully E side of lake
013	2807242	6317154	1897134	5755628		Small double box gully E side of lake
014	2806701	6316749	1896593	5755222		Roadside Outcrop
015	2806706	6316754	1896596	5755227		Roadside Outcrop
016	2806702	6316766	1896594	5755239		Roadside Outcrop
017	2806707	6316774	1896599	5755247		Roadside Outcrop
018	2806702	6316781	1896594	5755254		Roadside Outcrop
019	2806705	6316750	1896597	5755223		Roadside Outcrop
020	2806729	6316950	1896621	5755423		Bend in road SW side of Okaro
021	2806729	6316950	1896621	5755423		Above 020
022	2806729	6316950	1896621	5755423		Opposite side of road from 020
023	2806734	6316984	1896626	5755457		Roadside Outcrop
024	2806738	6316995	1896630	5755468		Drainage ditch in bend in road SW edge of lake
025	2806690	6317065	1896528	5755538		Roadside Outcrop
026	2807021	6317731	1896912	5755205		Deep gully on Landcorp property
027	2807045	6317590	1896936	5755064		Ridge N of Okaro on Landcorp property
028	2806658	6317797	1896549	5755270		Road cutting N of Landcorp underpass
029	2806833	6317859	1896724	5755333		Road cutting S of Landcorp underpass
030	2806658	6317797	1896549	5755270		See 2005/028
031	2806979	6317816	1896870	5756290		Landcorp Rotomahana property
032	2806981	6317829	1896872	5756303		Pit dug in gully on Landcorp property
033	2806973	6317840	1896864	5756314		Hole dug into lower flank of gully on Landcorp property
034	2806969	6317857	1896860	5756331		Hole dug into lower flank of gully on Landcorp property
035	2806971	6317839	1896862	5756313		Trench dug across small gully on Landcorp property
036	2806967	6317863	1896858	5756337		Hole dug into lower flank of gully on Landcorp property
037	2806935	6317485	1896826	5755968		Bank on lake shore
038	2806722	6316297	1896615	5754769		Landslide headscarp 200 m up Waimangu Rd from SH38
039	2806724	6316247	1896617	5754710		150 m up Waimangu Rd from SH38
040	2806709	6317301	1896600	5755774		Okaro picnic area N of carpark
041	2806608	6316762	1896500	5755234		Birchall property, near track cut
042	2806576	6316580	1896468	5755052		Birchall property, no Okaro Breccia
043	2806382	6316804	1896274	5755276		Birchall property, no Okaro Breccia
044	2806394	6316945	1896285	5755417		Birchall property, near track cut
045	2806286	6316926	1896178	5754758		Birchall property
046	2806284	6316942	1896175	5755414		Birchall property, near track cut

Lake Okaro: Explosions and Erosion

Outcrop	NZMG		NZTM		OU Samples	Description
	Easting	Northing	Easting	Northing		
047	2806182	6316866	1896073	5755338	OU75067; OU75968	Birchall property quarry
048	2806721	6317008	1896613	5755481		N of bend in road SW of lake Okaro
049	2806361	6317046	1896252	5755518		Silt-trap on Birchall property
050	2806341	6317034	1896232	5755596		Silt-trap on Birchall property
051	2806327	6317019	1896218	5755491		Silt-trap on Birchall property
052	2806306	6317007	1896197	5755479		Silt-trap on Birchall property
053	2806245	6317016	1896136	5755488		Birchall property, near track cut
054	2806105	6317129	1895996	5755601		Birchall property, near track cut
055	2806038	6317181	1895929	5755653		Birchall property, near track cut
056	2806228	6317087	1896119	5755559		Farm track in sheep paddock
057	2806212	6317079	1896103	5755551		Farm track in sheep paddock
058	2806196	6317110	1896087	5755582		Farm track in sheep paddock
059	2806182	6317118	1896073	5755590		Farm track in sheep paddock
060	2806250	6317083	1896141	5755555		Farm track in sheep paddock
061	2806296	6317085	1896187	5755557		Birchall property
062	2806540	6317249	1896431	5755722		Cutting in farm road behind house
063	2806533	6317260	1896424	5755733		Cutting in farm road behind house
064	2806472	6317311	1896363	5755784		Farm track cutting behind houses
065	2806443	6317467	1896334	5755940		Road cutting on Birchall property
066	2806455	6317468	1896346	5755941		Farm track cutting behind houses
067	2806480	6317486	1896371	5755959		Road cut
068	2807514	6316564	1897407	5755037		Lynskey farm cattle race
069	2806724	6316766	1896615	5755239		South side of lake at top of hill
070	2806799	6316770	1896691	5755243		Top of hill immediately S of Okaro
071	2807182	6317678	1897073	5756152		Gully, Landcorp Rotomahana property
072	2807164	6317638	1897055	5756112		Gully, Landcorp Rotomahana property
073	2807214	6317619	1897105	1756093		Gully, Landcorp Rotomahana property
074	2807238	6317618	1897129	5756092		Gully, Landcorp Rotomahana property
075	2807329	6317629	1897220	5756103		Gully, Landcorp Rotomahana property
076	2807063	6317559	1896954	5756033		Gully, Landcorp Rotomahana property
077	2806721	6316961	1896613	5755434		Road cut
078	2806632	6317791	1896523	5756264		Landcorp Rotomahana property, west of Okaro Road
079	2806619	6317835	1896510	5756308		Landcorp Rotomahana property, west of Okaro Road
080	2806602	6317887	1896492	5756360		Landcorp Rotomahana property, west of Okaro Road
081	2806606	6317919	1896496	5756392		Landcorp Rotomahana property, west of Okaro Road
082	2806610	6317918	1896500	5756391		Landcorp Rotomahana property, west of Okaro Road
083	2806617	6317920	1896507	5756393		Landcorp Rotomahana property, west of Okaro Road
AG01	2806685	6317014	1896577	5755487		Hand auger through topsoil, Birchall property
AG02	2806634	6317004	1896526	5755477		Hand auger through topsoil, Birchall property
AG03	2806584	6317008	1896476	5755481		Hand auger through topsoil, Birchall property
AG04	2806535	6317015	1896426	5755488		Hand auger through topsoil, Birchall property
AG05	2806487	6317001	1896378	5755473		Hand auger through topsoil, Birchall property
AG06	2806433	6317015	1896324	5755487		Hand auger through topsoil, Birchall property
AG07	2806386	6317003	1896277	5755475		Hand auger through topsoil, Birchall property
AG08	2806337	6316996	1896228	5755468		Hand auger through topsoil, Birchall property
AG09	2806285	6316977	1896176	5755449		Hand auger through topsoil, Birchall property
AG10	2806238	6317049	1896129	5755522		Hand auger through topsoil, Birchall property
AG11	2806181	6317120	1896072	5755592		Hand auger through topsoil, Birchall property

Lake Okaro: Explosions and Erosion

Outcrop	NZMG		NZTM		OU Samples	Description
	Easting	Northing	Easting	Northing		
AG12	2806098	6317132	1895989	5755604		Hand auger through topsoil, Birchall property
AG13	2806034	6317184	1895925	5755656		Hand auger through topsoil, Birchall property
AG14	2806196	6316878	1896087	5755350		Hand auger through topsoil, Birchall property
BL01	2806951	6317905	1896842	5756379		Landcorp Rotomahana valley
BL02	2806951	6317879	1896842	5756353		Landcorp Rotomahana valley
BL03	2806951	6317853	1896842	5756327		Landcorp Rotomahana valley
BL04	2806953	6317837	1896844	5756311		Landcorp Rotomahana valley
BL05	2806954	6317828	1896845	5756302		Landcorp Rotomahana valley
BL06	2806956	6317823	1896847	5756297		Landcorp Rotomahana valley
BL07	2806957	6317815	1896848	5756289		Landcorp Rotomahana valley
BL08	2806960	6317803	1896851	5756277		Landcorp Rotomahana valley
BL09	2806962	6317793	1896853	5756267		Landcorp Rotomahana valley
BL10	2806966	6317773	1896857	5756256		Landcorp Rotomahana valley
V1P1	2806883	6317873	1896774	5756347		Landcorp Rotomahana valley
V1P2	2806907	6317896	1896798	5756370		Landcorp Rotomahana valley
V2P1	2806975	6317884	1896866	5756358		Landcorp Rotomahana valley
Z-a	2806721	6316955	1896613	5755428	OU75041 to OU75048	Roadcut, SW Lake
Z-b	2806721	6316950	1896613	5755423	OU75049 to OU75056	Roadcut, SW Lake
Z-c	2806721	6316947	1896613	5755420	OU75057 to OU75066	Roadcut, SW Lake

Lake Okaro: Explosions and Erosion

8.4 Appendix D – Auger Hole Data & Locations

Grid coordinates in GD2000 projection

z = GPS elevation above mean sea level

d = depth to base of Rotomahana Mud or depth AD1886 soil horizon interception

Baseline				
Hole #	mE	mN	z	dNotes
BL01	1896842	5756379	437	0.63 Thin 1886 - eroded?
BL02	1896842	5756353	435	0.95 Waimangu deposits encountered
BL03	1896842	5756327	433	0.68 Thin Waimangu/1886
BL04	1896844	5756311	432	0.58 Top of slope
BL05	1896845	5756302	427	0.37 Upper slope
BL06	1896847	5756297	425	0.58 Middle slope
BL07	1896848	5756289	423	0.50 Lower slope
BL08	1896851	5756277	419	>0.95 Reworked Waimangu, Slope wash
BL09	1896853	5756267	418	>0.95 Base of slope/slope wash. Reworked Waimangu. Fine-depleted Rotomahana
BL10	1896857	5756256	416	>0.95 Base of slope/slope wash. Reworked Waimangu. Fine-depleted Rotomahana

Valley 1				
Set 1				Notes
V1P1	Rill	Inter-rill		1896774mE, 5756347mN
Set 1 Top	0.55	0.9		Rill at grid coordinates; inter-rill to true left
Set 1 Middle	0.73	0.9		1 metre further down rill from grid coordinates
Set 1 Bottom	0.79	0.9		2 metres further down rill from grid coordinates

Set 2				
V1P2	Rill	Inter-rill		Notes
				1896798mE, 5756370mN
Set 2 Top	0.60	0.90		Rill at grid coordinates; inter-rill to true left
Set 2 Middle	0.69	0.90		1 metre further down rill from grid coordinates
Set 2 Bottom	0.80	0.90		2 metres further down rill from grid coordinates

Valley 2				
V2P1	Rill	Inter-rill		Notes
				1896866mE, 5756358mN
1	0.70	0.9		Rill at grid coordinates; inter-rill to true right
2	0.65	0.9		1 metre further down rill from grid coordinates

Lake Okaro: Explosions and Erosion

8.5 Appendix E – Grainsize Analysis Data

OU Number	OU75042	OU75043	OU75044	OU75045	OU75046	OU75047	OU75048	OU75049	OU75050
Field Number	z02	z03	z04	z05	z06	z07	z08	z09	z10
Elevation (m)	0.05	0.5	1	1.5	2	2.2	2.5	2.5	3
Unit	Okaro A	Okaro A	Okaro A	Okaro A	Okaro A	Okaro B	Okaro B	Okaro B	Okaro B
λ Interval	Weight Percent								
-4.00	4.77	1.40	1.12	4.14	0.00	8.93	2.84	0.00	8.71
-3.50	0.57	0.00	3.13	1.21	0.00	3.82	7.72	1.06	5.43
-3.00	2.11	3.27	2.12	5.19	1.45	5.00	1.58	5.62	7.48
-2.50	2.86	4.93	4.01	3.92	1.46	5.70	6.94	7.34	8.75
-2.00	3.21	2.99	4.10	3.64	2.50	5.84	7.57	7.90	7.30
-1.50	4.33	3.81	3.44	3.92	2.91	9.56	6.88	5.84	10.90
-1.00	4.70	4.89	4.37	3.94	3.80	6.85	8.64	7.45	7.43
-0.50	8.31	8.53	7.16	6.68	7.02	9.09	9.75	9.55	9.20
0.00	10.77	11.28	9.07	7.96	9.85	10.44	12.03	13.39	10.17
0.50	11.02	10.16	8.99	7.51	9.99	7.46	7.72	9.30	6.30
1.00	10.37	10.61	10.09	8.57	12.18	7.38	7.72	9.40	5.93
1.50	6.16	7.36	7.66	6.16	9.36	4.89	4.96	6.43	3.33
2.00	6.93	7.69	7.26	7.01	8.73	3.66	4.00	5.25	2.68
2.50	5.74	5.60	5.48	5.59	6.73	2.42	2.59	3.27	1.68
3.00	4.46	4.58	4.87	4.39	5.37	2.23	2.35	2.46	1.52
3.50	3.75	3.34	4.55	3.85	3.97	1.58	1.66	1.54	0.92
4.00	2.46	2.77	3.75	4.72	3.58	1.50	1.55	1.42	0.81
4.50	1.45	1.33	1.81	2.42	2.22	0.95	1.03	0.90	0.51
5.00	1.34	1.25	1.76	2.43	1.99	0.83	0.81	0.63	0.34
5.50	1.25	1.16	1.60	2.18	1.78	0.62	0.57	0.42	0.20
6.00	0.98	0.89	1.15	1.49	1.37	0.38	0.34	0.25	0.11
6.50	0.78	0.69	0.83	1.04	1.11	0.26	0.24	0.17	0.08
7.00	0.51	0.45	0.52	0.62	0.76	0.17	0.15	0.11	0.05
7.50	0.35	0.31	0.34	0.41	0.55	0.12	0.11	0.08	0.04
8.00	0.21	0.19	0.20	0.24	0.35	0.08	0.07	0.05	0.03
8.50	0.16	0.14	0.15	0.19	0.27	0.07	0.06	0.04	0.03
9.00	0.11	0.09	0.10	0.13	0.19	0.05	0.04	0.03	0.02
9.50	0.08	0.07	0.08	0.11	0.15	0.04	0.04	0.03	0.02
10.00	0.07	0.06	0.07	0.09	0.10	0.03	0.03	0.02	0.01
10.50	0.06	0.05	0.06	0.08	0.09	0.02	0.02	0.02	0.01
11.00	0.05	0.04	0.05	0.06	0.07	0.01	0.01	0.01	0.00
11.50	0.04	0.03	0.04	0.04	0.05	0.00	0.00	0.00	0.00
Remainder	0.08	0.07	0.08	0.08	0.09	0.00	0.00	0.00	0.00
Total	100.00	100.00	100.00	100.00	100.00	100.00	100.00	100.00	100.00

Merger of sieve and Coulter data between 4λ and 4.5λ

Raw data in Excel spreadsheet “Grainsize Data” on accompanying CD-ROM

Graphical Statistics and Cumulative Probability plots can be found in Word documents in “Grainsize Reports” folder on accompanying CD-ROM listed by field number

Lake Okaro: Explosions and Erosion

OU Number	OU75051	OU75052	OU75053	OU75054	OU75055	OU75056	OU75057	OU75058	OU75059
Field Number	z11	z12	z13	z14	z15	z16	z17	Z18	z19
Elevation (m)	3.5	4	4.5	5	5.25	5.75	6.25	6.75	7.25
Unit	Okaro B	Okaro B	Okaro B	Okaro B	Okaro B	Okaro B	Okaro B	Okaro B	Okaro B
λ Interval	Weight Percent								
-4.00	0.00	4.20	0.00	0.00	9.05	4.94	0.00	5.42	6.31
-3.50	6.90	2.13	2.58	9.32	6.25	1.66	4.39	11.15	10.53
-3.00	4.45	4.06	1.66	4.94	7.34	2.47	5.59	3.54	11.71
-2.50	8.44	6.18	5.07	5.52	5.73	4.45	6.91	9.09	8.57
-2.00	9.29	5.58	9.07	7.05	3.23	9.17	10.90	9.59	8.79
-1.50	11.76	7.31	13.00	5.01	5.93	12.71	12.75	7.06	8.56
-1.00	10.15	9.29	12.50	6.95	6.03	10.23	9.86	6.58	8.52
-0.50	11.28	12.13	11.99	8.80	9.38	11.17	9.83	8.19	8.85
0.00	8.85	12.61	9.70	11.54	8.75	9.10	8.01	8.39	7.72
0.50	6.93	9.35	7.41	7.73	8.71	6.97	5.90	8.66	5.32
1.00	6.92	8.76	6.91	7.37	7.60	6.57	5.75	7.06	4.99
1.50	3.99	5.08	4.94	4.92	4.47	4.45	3.88	4.52	3.05
2.00	3.47	3.87	3.91	4.41	4.03	3.79	3.55	3.46	2.22
2.50	2.24	2.47	2.75	3.12	2.84	2.66	2.42	2.12	1.33
3.00	1.59	1.96	2.34	3.02	2.54	2.34	2.42	1.74	1.07
3.50	1.09	1.40	1.74	2.49	1.95	1.85	1.89	1.22	0.81
4.00	0.93	1.20	1.43	2.38	1.86	1.75	1.83	0.90	0.68
4.50	0.58	0.80	1.00	1.67	1.47	1.16	1.33	0.46	0.31
5.00	0.40	0.59	0.71	1.34	1.07	0.92	1.06	0.31	0.21
5.50	0.25	0.37	0.45	0.91	0.68	0.62	0.69	0.19	0.14
6.00	0.14	0.20	0.26	0.52	0.37	0.35	0.37	0.10	0.08
6.50	0.10	0.13	0.17	0.33	0.24	0.22	0.23	0.07	0.06
7.00	0.07	0.08	0.11	0.19	0.13	0.13	0.13	0.04	0.04
7.50	0.05	0.06	0.08	0.12	0.09	0.08	0.09	0.03	0.03
8.00	0.03	0.04	0.05	0.08	0.06	0.05	0.06	0.02	0.02
8.50	0.03	0.04	0.05	0.06	0.05	0.04	0.05	0.02	0.02
9.00	0.02	0.03	0.04	0.05	0.04	0.03	0.04	0.02	0.01
9.50	0.02	0.03	0.03	0.04	0.03	0.03	0.03	0.01	0.01
10.00	0.01	0.02	0.02	0.04	0.03	0.02	0.03	0.01	0.01
10.50	0.01	0.01	0.02	0.03	0.02	0.02	0.02	0.01	0.01
11.00	0.00	0.01	0.01	0.02	0.02	0.01	0.01	0.00	0.00
11.50	0.00	0.00	0.00	0.01	0.01	0.01	0.01	0.00	0.00
Remainder	0.00	0.00	0.00	0.01	0.01	0.00	0.01	0.00	0.00
Total	100.00	100.00	100.00	100.00	100.00	100.00	100.00	100.00	100.00

Merger of sieve and Coulter data between 4λ and 4.5λ

Raw data in Excel spreadsheet "Grainsize Data" on accompanying CD-ROM

Graphical Statistics and Cumulative Probability plots can be found in Word documents in "Grainsize Reports" folder on accompanying CD-ROM listed by field number

Lake Okaro: Explosions and Erosion

OU Number	OU75060	OU75061	OU75062	OU75063	OU75064	OU75065	OU75066	OU75067
Field Number	z20	z21	z22	z23	z24	z25	z26	047C
Elevation (m)	7.75	8.25	8.75	9.25	9.75	10.25	10.75	
Unit	Okaro B	Okaro B	Okaro C	Earthquake Flat				
# Interval	Weight Percent							
-4.00	14.98	9.00	6.29	1.29	2.66	4.62	0.00	0.00
-3.50	9.79	6.70	2.80	4.51	5.35	3.94	0.00	2.79
-3.00	7.29	6.07	4.82	4.61	5.95	5.56	0.00	1.81
-2.50	10.39	8.67	6.79	7.15	10.02	5.71	0.00	2.30
-2.00	6.76	7.07	9.03	11.07	10.42	7.84	0.00	3.18
-1.50	7.62	8.46	12.14	11.58	10.45	10.38	0.11	3.94
-1.00	7.13	8.37	10.45	10.76	10.43	11.10	0.82	4.85
-0.50	8.07	10.26	11.45	11.61	10.77	12.51	3.31	5.86
0.00	7.00	9.25	9.33	9.82	8.61	10.29	6.52	7.50
0.50	5.53	7.36	7.06	7.24	6.37	7.48	9.59	6.84
1.00	5.12	6.53	6.35	6.64	5.46	6.84	14.41	8.12
1.50	2.97	3.95	4.10	4.42	3.67	4.20	14.73	6.07
2.00	2.42	2.92	3.12	3.33	2.75	3.26	14.68	7.00
2.50	1.47	1.73	1.96	1.93	1.78	1.85	9.53	5.91
3.00	1.16	1.21	1.51	1.47	1.53	1.48	7.74	6.68
3.50	0.78	0.84	0.99	0.94	1.08	0.97	4.87	5.97
4.00	0.65	0.62	0.78	0.74	0.93	0.81	4.28	5.81
4.50	0.27	0.32	0.30	0.27	0.52	0.36	2.47	5.43
5.00	0.21	0.24	0.20	0.19	0.42	0.26	1.98	9.94
5.50	0.13	0.15	0.13	0.13	0.29	0.17	1.50	
6.00	0.07	0.08	0.09	0.08	0.17	0.10	1.01	
6.50	0.05	0.05	0.07	0.06	0.11	0.07	0.75	
7.00	0.03	0.03	0.06	0.04	0.07	0.05	0.50	
7.50	0.02	0.02	0.05	0.03	0.05	0.04	0.36	
8.00	0.02	0.02	0.04	0.02	0.04	0.03	0.23	
8.50	0.02	0.02	0.03	0.02	0.03	0.03	0.19	
9.00	0.01	0.01	0.03	0.02	0.02	0.02	0.14	
9.50	0.01	0.01	0.02	0.01	0.02	0.02	0.12	
10.00	0.01	0.01	0.02	0.01	0.02	0.01	0.08	
10.50	0.00	0.01	0.01	0.01	0.01	0.01	0.05	
11.00	0.00	0.00	0.01	0.00	0.00	0.00	0.03	
11.50	0.00	0.00	0.00	0.00	0.00	0.00	0.01	
Remainder	0.00	0.00	0.00	0.00	0.00	0.00	0.00	
Total	100.00	100.00	100.00	100.00	100.00	100.00	100.00	100.00

Merger of sieve and Coulter data between 4λ and 4.5λ

Raw data in Excel spreadsheet "Grainsize Data" on accompanying CD-ROM

Graphical Statistics and Cumulative Probability plots can be found in Word documents in "Grainsize Reports" folder on accompanying CD-ROM listed by field number

8.6 Appendix F – X-Ray Diffraction Data Summary

Sample	Quartz	Plagioclase Series	K Feldspar Series	Biotite	Muscovite	Sericite	Kaolinite	Montmorillonite	Zeolite	Jarosite
OU75042	x	x		x						
OU75043	x	x			x					
OU75044	x	x								
OU75045	x	x	x			x				
OU75046	x		x		x					
OU75047	x		x			x				
OU75048	x		x			x				
OU75049	x	x				x	x			
OU75050	x		x		x	x		x		
OU75051	x		x				-	x		
OU75052	x	x					x	x		
OU75053	x		x			x	x			
OU75054	x		x				x	x		
OU75055	x	x					x	x		
OU75056	x	x					x			
OU75057	x	x					x			
OU75058	x		x				x			
OU75059	*		x				x	x		
OU75060	*		x				x	x		
OU75061	x								x	x
OU75062	x	x						x		x
OU75063	x	x					x	x		
OU75064	*		x				x			
OU75065	x		x				x	x		
OU75066	x		x	x			x			

x = Present

- = Present in association with Montmorillonite

* = Present as Quartz and Opal

XRD reports can be found in folder titled “X-Ray Diffraction Reports” on accompanying CD-ROM

8.7 Appendix G – Electron Microprobe Analysis Data

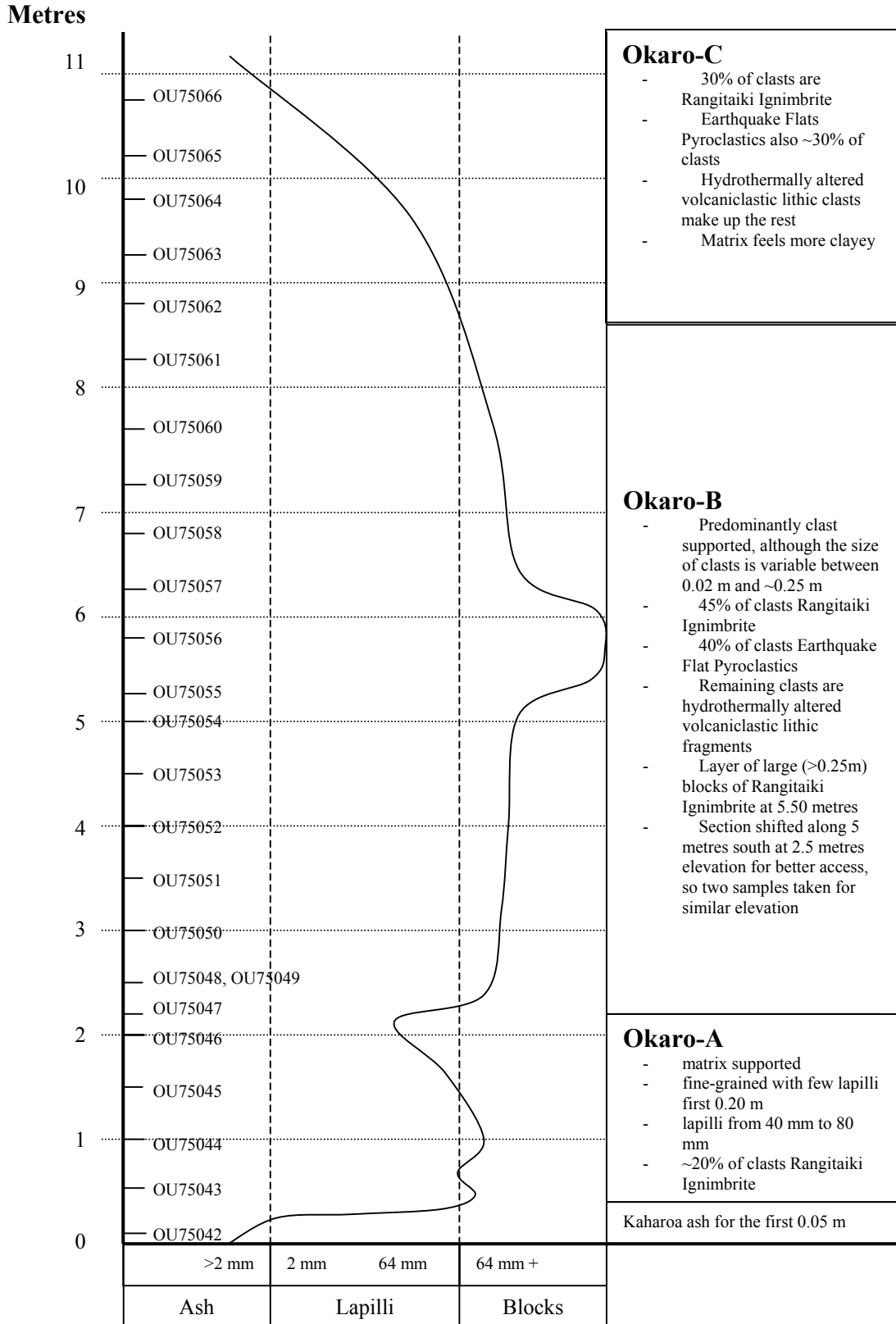
	pm-g1s1	pm-g1s3	pm-g2s3	pm-g2s4	pm-g3s1	pm-g3s3	pm-g2s6	bx-g1s1	bx-g1s2	bx-g3s2	bx-g2s3	* bx-g6s1	* bx-g6s3	* bx-g6s4	* bx-g6s5
SiO ₂	76.52	76.30	77.48	77.77	78.86	77.11	77.48	77.08	77.41	77.63	77.87	80.35	79.38	80.98	77.87
TiO	0.09	0.09	0.09	0.09	0.09	0.09	0.09	0.06	0.06	0.10	0.09	0.09	0.08	0.09	0.05
Al ₂ O ₃	11.88	12.15	12.05	12.06	12.41	12.36	11.99	12.07	12.00	12.08	12.25	10.11	11.00	12.67	12.30
FeO	0.90	0.80	0.89	0.80	0.90	0.89	0.85	0.85	0.80	0.89	0.76	0.81	0.80	0.85	0.89
MnO	0.03	0.01	0.06	0.06	0.00	0.03	0.05	0.04	0.06	0.01	0.05	0.00	0.03	0.07	0.03
MgO	0.07	0.06	0.08	0.06	0.08	0.08	0.08	0.06	0.05	0.05	0.08	0.08	0.07	0.08	0.07
CaO	0.73	0.72	0.73	0.71	0.73	0.74	0.70	0.72	0.70	0.72	0.75	0.61	0.66	0.71	0.75
Na ₂ O	3.62	3.50	3.43	3.47	3.61	3.38	3.53	3.37	3.45	3.38	3.41	2.77	3.11	1.68	3.04
K ₂ O	4.2	4.26	4.33	4.40	4.22	4.06	4.39	4.31	4.27	4.27	4.28	3.65	3.87	3.53	4.19
Total	98.04	97.89	99.14	99.42	100.90	98.74	99.16	98.56	98.80	99.13	99.54	98.47	99.00	100.66	99.19

All iron reported as FeO

Yellow highlighted samples are contaminated by either quartz oversaturation due to the electron beam burning through the sample, or alkali migration from electron beam intensity causing Na and K to abandon the crystal matrix

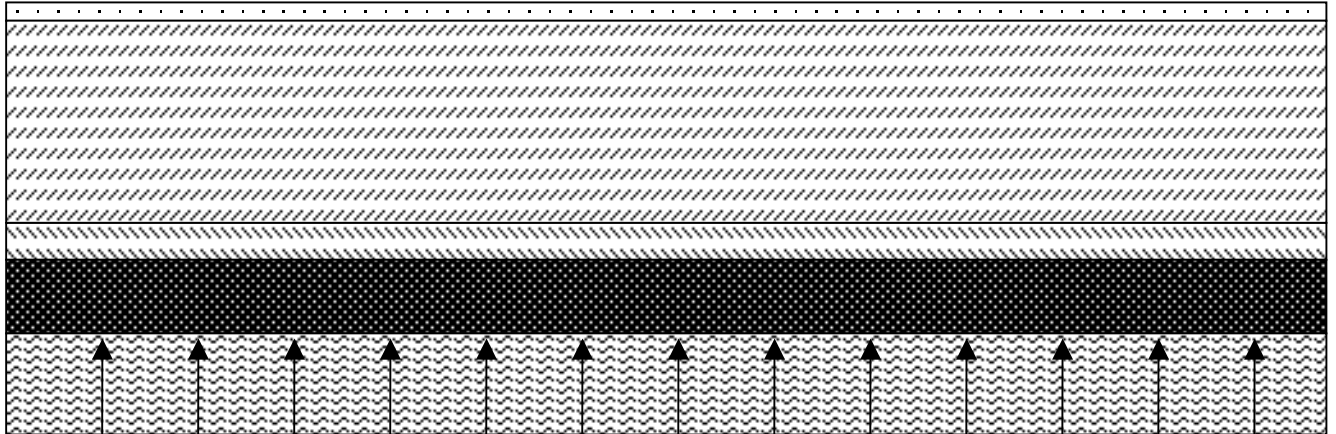
CPIW Normative calculations in Excel file “CPIW Norms for Microprobe Samples” on accompanying CD-ROM

8.8 Appendix H – Composite Measured Section Through Okaro-Breccia

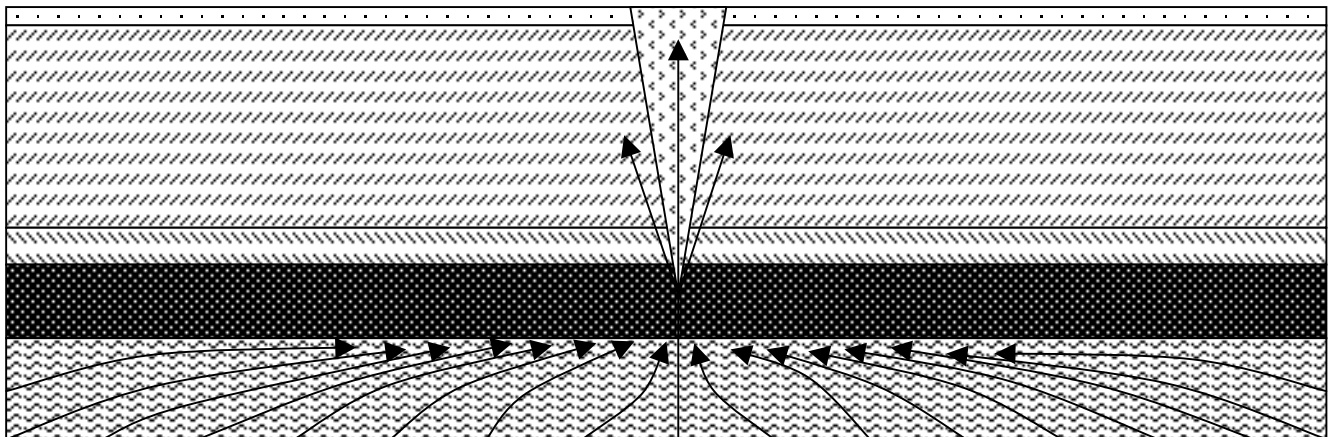


8.9 Appendix I – Schematic Interpretation of Eruption for the Okaro-A and -B Deposits and the Formation of Lake Okaro

This interpretation assumes that the heat required to generate the steam powering the eruption came from a basaltic dyke arrested at depth (as discussed in Section 5) resulting in a phreatic eruption. No direct hydrothermal system interaction is assumed for this event.

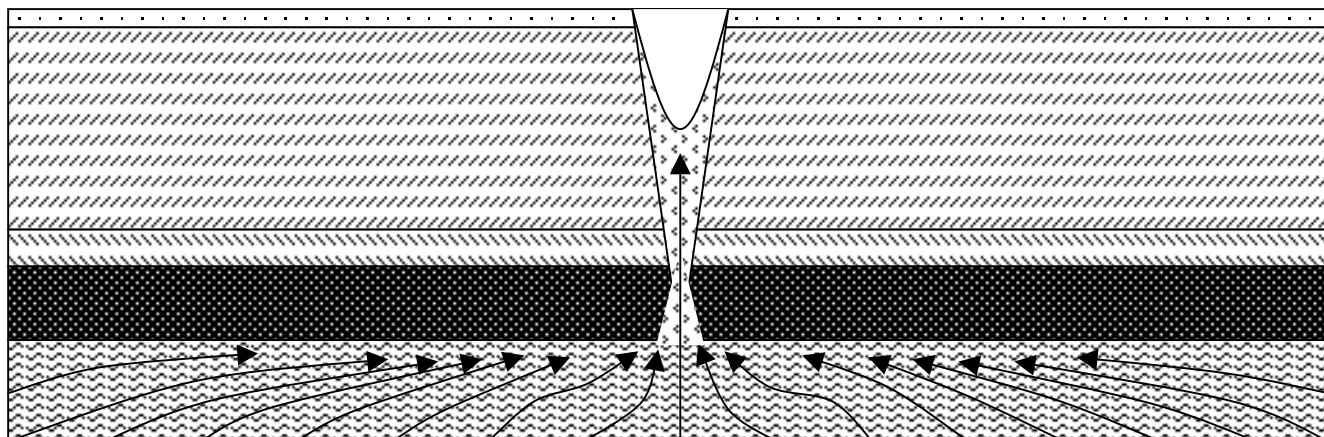


Step 1 Steam and heated groundwater from basaltic intrusion rises toward the surface and encounters cap of Rangitaiki Ignimbrite. Pressure starts to increase, as no release is available.

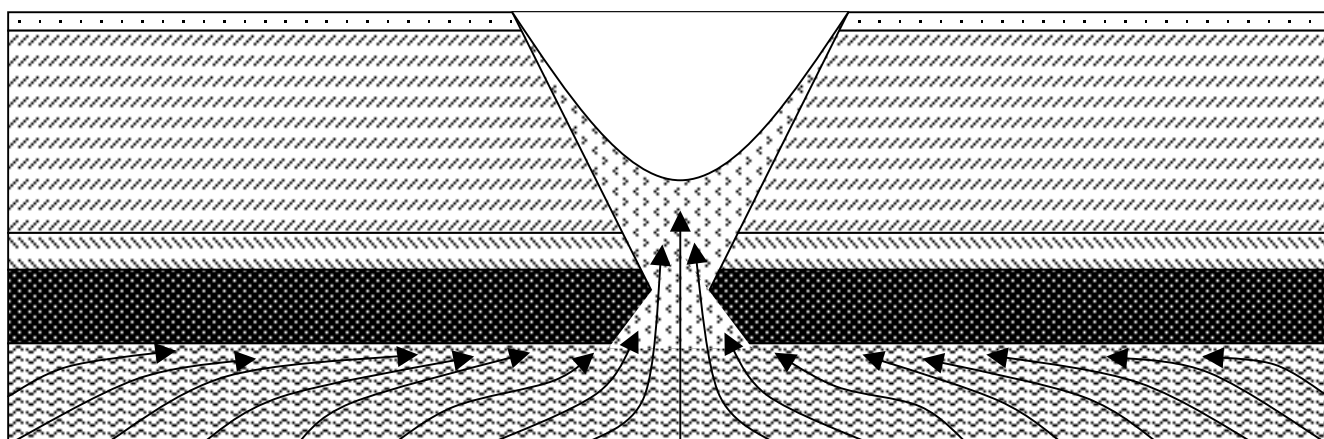


Step 2 Rangitaiki Ignimbrite fails allowing steam to escape. A brecciated zone forms above the failure point, fragmenting the Rangitaiki Ignimbrite further and starts mixing the Rangitaiki Ignimbrite with the Earthquake Flat Pyroclastics. Okaro-A starts to be deposited, with the base of the deposit being composed of predominantly Earthquake Flat Pyroclastics-derived material.

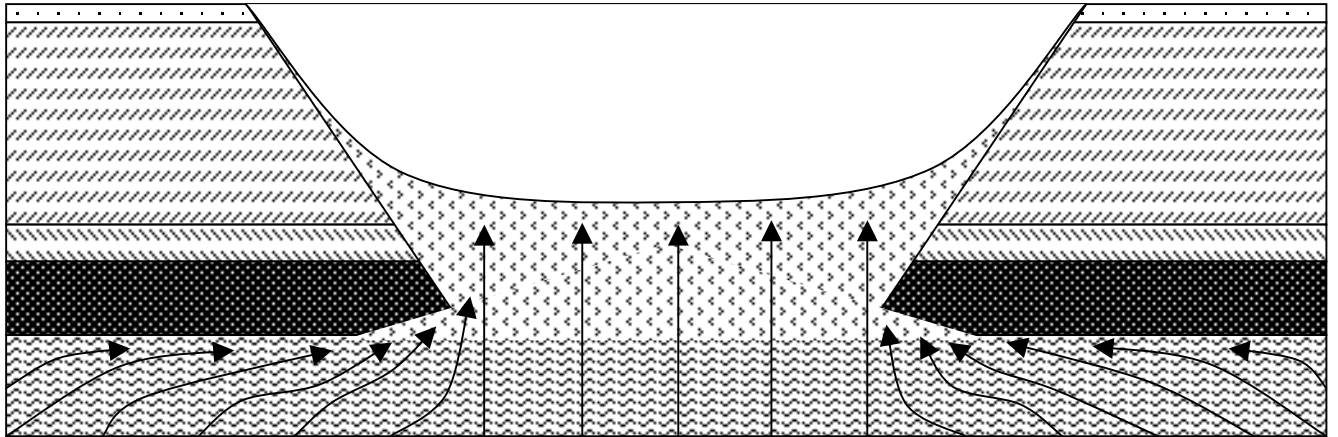
Lake Okaro: Explosions and Erosion



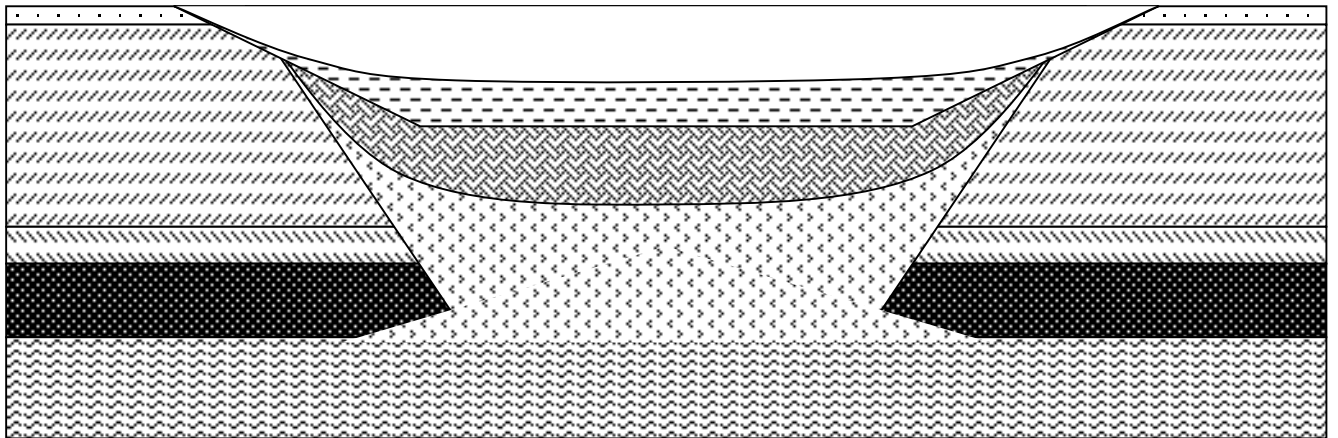
Step 3: Escaping steam expands rupture in Rangitaiki Ignimbrite. Eruption Vent forms allowing material from deeper down to be deposited. Large blocks remain in the vent, while small blocks (<100mm) ejected. Okaro-A deposited in the manner.



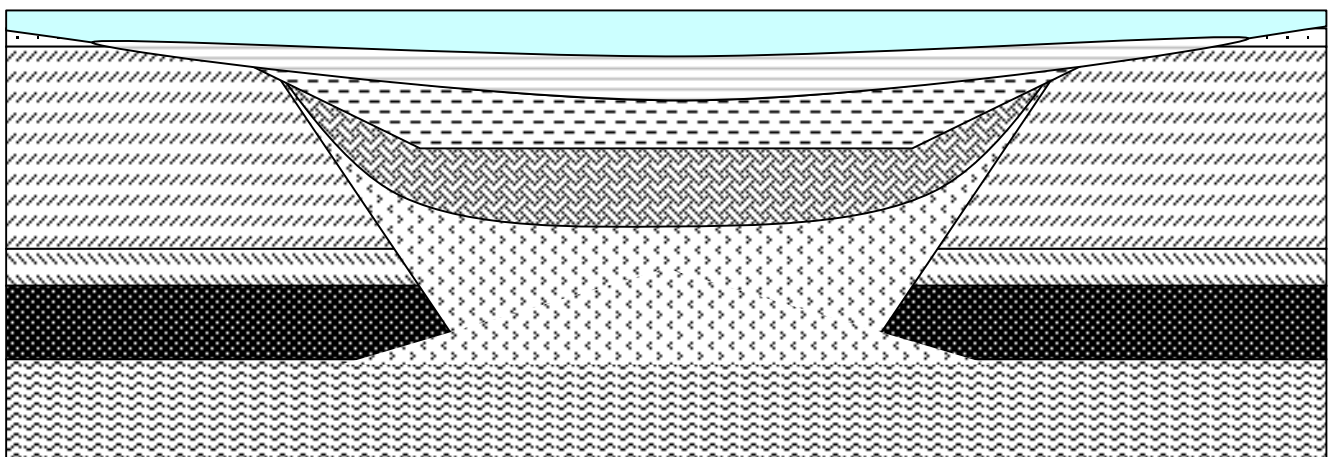
Step 4: As more steam is released, the crater becomes deeper and steeper. Vent slopes fail and previously ejected material collapses back into the crater to be thrown out again. Large blocks (>100mm) become common in the ejecta. Deposition of Okaro-B takes place. Okaro-C eruptions start to the north and add hydrothermally altered material into the crater.



Step 5: Okaro-B phase continues until the pressure is equalized. Vent is widened considerably, with the diameter being roughly four times the depth.



Step 6: Slumping of vent walls partially fills in the vent (hatched fill). Deposition of Okaro-C material adds to this.



Step 7: Crater is filled with water from a blocked stream; Lake Okaro forms. Aggradation of the lake floor from stream deposition, as well as with Rotomahana Mud from the AD1886 Tarawera eruption brings lake to present observed depth.

8.10 Appendix J – Paleogeographic Interpretation of the Area Now Occupied by Lake Okaro

